ARTICLE

https://doi.org/10.1038/s41586-019-1515-6

There are amendments to this paper

Temporal plasticity of apical progenitors in the developing mouse neocortex

Polina Oberst[1,3], Sabine Fièvre[1], Natalia Baumann[1], Cristina Concetti[1,4], Giorgia Bartolini[1] & Denis Jabaudon[1,2]*

The diverse subtypes of excitatory neurons that populate the neocortex are born from apical progenitors located in the ventricular zone. During corticogenesis, apical progenitors sequentially generate deep-layer neurons followed by superficial-layer neurons directly or via the generation of intermediate progenitors. Whether neurogenic fate progression necessarily implies fate restriction in single progenitor types is unknown. Here we specifically isolated apical progenitors and intermediate progenitors, and fate-mapped their respective neuronal progeny following heterochronic transplantation into younger embryos. We find that apical progenitors are temporally plastic and can re-enter past molecular, electrophysiological and neurogenic states when exposed to an earlier-stage environment by sensing dynamic changes in extracellular Wnt. By contrast, intermediate progenitors are committed progenitors that lack such retrograde fate plasticity. These findings identify a diversity in the temporal plasticity of neocortical progenitors, revealing that some subtypes of cells can be untethered from their normal temporal progression to re-enter past developmental states.

During neocorticogenesis, distinct subtypes of neurons are sequentially generated and can be distinguished by their laminar location, connectivity and gene-expression programs[1,2]. They are born from distinct subtypes of progenitors including apical progenitors (APs) and intermediate progenitors (IPs), the molecular identity and overall neurogenic competence of which progress with time. Initially, APs give rise to deep-layer-type (DL) neurons, whereas they subsequently generate superficial-layer-type (SL) neurons[3–8]. Similarly, early IPs initially generate both DL and SL neurons, but subsequently only give rise to SL neurons[7,9–11]. Although the aggregate ability of mixed progenitor populations to generate earlier-born types of neurons when transplanted in a younger host appears to be lost[12,13], whether individual subtypes of progenitors can revert to previous temporal states in response to environmental cues remains unknown. Here we isolate specific populations of cortical progenitors and probe their fate plasticity using heterochronic transplantation into younger hosts.

Late-born APs are competent to generate DL neurons

To investigate the fate plasticity of APs, we performed FlashTag pulse-labelling in CAG-mRFP1 donor mice and immediately isolated FlashTag$^+$ cells using flow cytometry (FlashTag labels APs on the basis of their juxtaventricular location)[14,15]. FlashTag$^+$ APs were transplanted into wild-type host embryos by intraventricular injection[16–18] (Fig. 1, Extended Data Fig. 1a), and the fate of their (RFP$^+$) neuronal progeny was determined on postnatal day (P)7, once migration is complete. We first performed isochronic AP transplantations at embryonic day (E)15.5 ($AP_{15\rightarrow15}$), when SL neurons (that is, neurons in layer (L) 4 and L2–L3) are formed, and at E12.5 ($AP_{12\rightarrow12}$), when DL neurons (that is, L6 and L5) are generated[1,2]. Using these two conditions as controls, we then heterochronically transplanted E15.5 APs into E12.5 host embryos ($AP_{15\rightarrow12}$). Integration of transplanted APs occurred at single sites, and post-mitotic neuron migration followed a physiological time course to form single 'oligoclones' (Extended Data Fig. 1b–d, Supplementary Note 1). At P7, both $AP_{15\rightarrow15}$ and $AP_{12\rightarrow12}$ had generated daughter neurons with appropriate laminar locations: $AP_{15\rightarrow15}$ gave rise to SL neurons whereas $AP_{12\rightarrow12}$ gave rise to DL and SL neurons, consistent with the sequential production of DL followed by SL neurons (Fig. 1b, c, Extended Data Fig. 2, and Supplementary Table 1). Unlike $AP_{15\rightarrow15}$ daughter neurons, $AP_{15\rightarrow12}$ daughter neurons were located in both DL and SL, as found for $AP_{12\rightarrow12}$ (Fig. 1d–g, Extended Data Fig. 3, Supplementary Table 1, Supplementary Note 1), which suggests that the neurogenic competence of AP_{15} is temporally plastic. The molecular identity of $AP_{15\rightarrow12}$ daughter neurons was congruent with their laminar position, as assessed using TBR1 (a marker of L6 neurons), CTIP2 (a marker of L5 neurons) and CUX1 (a marker of L2–L4 neurons) (Fig. 2a–c, Extended Data Fig. 4a–c). Axonal projections matched these laminar and molecular features: in contrast to $AP_{15\rightarrow15}$ progeny, which send axons to intracortical but not to subcerebral targets[1], $AP_{15\rightarrow12}$ progeny also projected subcerebrally, similar to $AP_{12\rightarrow12}$ daughter neurons (Fig. 2d). Together, these data reveal an embryonic-age-appropriate and congruous respecification of the laminar, molecular and hodological identity of $AP_{15\rightarrow12}$ daughter neurons.

Molecular and cellular respecification of $AP_{15\rightarrow12}$

In contrast to $AP_{15\rightarrow12}$, the small population of neurons that were being generated in the donor at the time of isolation ($N_{15\rightarrow12}$) did not show fate plasticity, pointing towards a pre-mitotic rather than post-mitotic respecification process (Extended Data Fig. 4d, e, Supplementary Note 2). To identify changes in $AP_{15\rightarrow12}$ cellular states, we first investigated their molecular identity by performing Patch-seq RNA sequencing[19,20] of visually identified RFP$^+$ juxtaventricular cells (Fig. 3a, b). This approach revealed that $AP_{15\rightarrow12}$ repress AP_{15}-type transcriptional programs and re-express AP_{12}-type transcriptional programs, and identified dynamically regulated genes following heterochronic transplantation (Fig. 3c, d, Extended Data Fig. 5a–d, Extended Data Table 1). Re-induced transcripts included the Wnt-pathway regulator *Tcf7l1*—which represses neuronal differentiation and increases self-renewal in cortical APs[21]—and the polycomb repressive complex 2 (PRC2) methyltransferase *Ezh2*—a critical regulator of the progression of AP neurogenic competence[8,22] and itself a target of the Wnt pathway[23]. Because Wnt signalling is normally active in an early–high to late–low gradient in the developing cortex[24,25], transcriptional

[1]Department of Basic Neurosciences, University of Geneva, Geneva, Switzerland. [2]Clinic of Neurology, Geneva University Hospital, Geneva, Switzerland. [3]Present address: Center for Stem Cell Biology, Memorial Sloan Kettering Cancer Center, New York, NY, USA. [4]Present address: Institute of Neuroscience, ETH Zürich, Schwerzenbach, Switzerland. *e-mail: denis.jabaudon@unige.ch

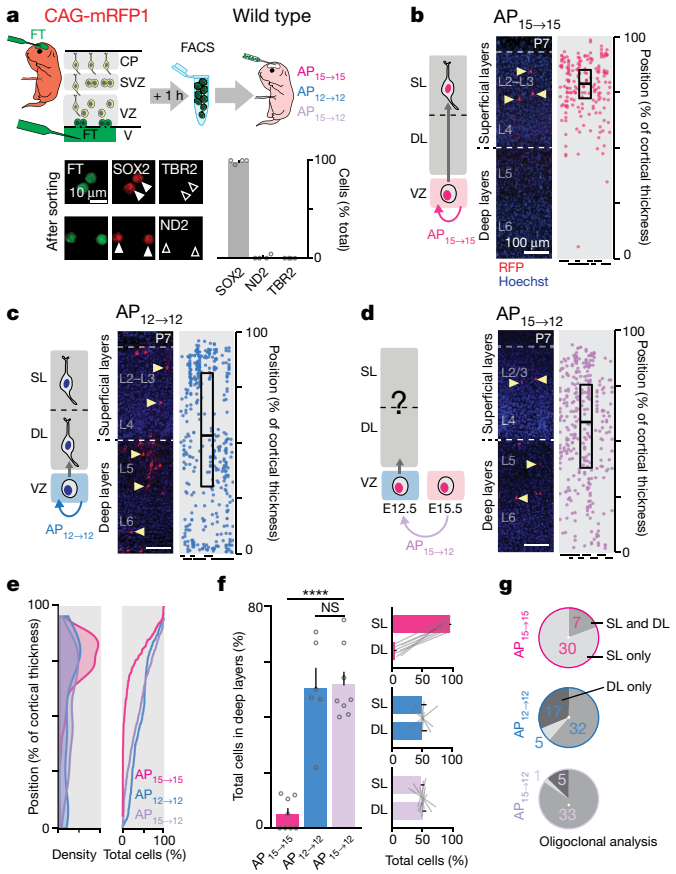

Fig. 1 | E15.5 APs remain competent to generate earlier-born deep-layer neurons. a, Top, schematic of the AP isolation and transplantation procedure. Bottom, donor cells consist essentially of $SOX2^+$ APs. TBR2, IP marker; ND2, NEUROD2 (neuronal marker). Data are mean ± s.e.m.; $n = 4$ coverslips per group. **b**, Isochronically transplanted E15.5 APs ($AP_{15\rightarrow15}$) generate SL neurons. $n = 8$ experimental litters. **c**, Isochronically transplanted E12.5 APs ($AP_{12\rightarrow12}$) give rise to DL and SL neurons. $n = 6$ experimental litters. **d**, E15.5 APs transplanted into an E12.5 host ($AP_{15\rightarrow12}$) give rise to DL and SL neurons. $n = 8$ experimental litters. Box plots in **b**–**d** indicate median and interquartile range. **e**, Radial distribution of daughter neurons at P7. **f**, Left, fraction of daughter neurons in DL at P7. One-way analysis of variance (ANOVA) with post hoc Tukey test. Right, modal distribution of daughter neurons in SL versus DL. Data reused from **b**–**d**; data are mean ± s.e.m. **g**, Oligoclonal integration-site analysis of the laminar distribution of daughter neurons (Extended Data Fig. 1b). V, ventricle. NS, not significant, $^{****}P < 0.0001$. In **b**–**d**, circles represent individual cells, vertically aligned by single integration sites. Dashes delineate individual experimental litters.

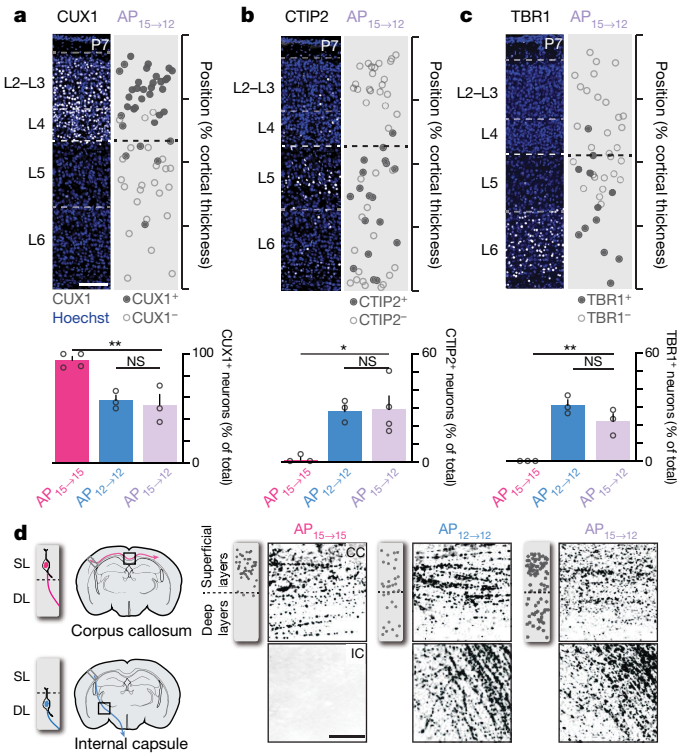

Fig. 2 | Embryonic-age-dependent molecular features and connectivity of $AP_{15\rightarrow12}$ daughter neurons. a, Levels of CUX1, an SL neuron marker, are lower in DL $AP_{15\rightarrow12}$ daughter neurons. Hoechst, nuclear stain. Scale bar, 100 μm. **b**, Expression of CTIP2, a DL neuron marker, is increased in DL $AP_{15\rightarrow12}$ daughter neurons. **c**, Expression of TBR1, a DL neuron marker, are increased in DL $AP_{15\rightarrow12}$ daughter neurons. **a**–**c**, One-way ANOVA with post hoc Tukey test; data are mean ± s.e.m.; $n = 4$ experimental litters ($AP_{15\rightarrow15}$ CUX1), 3 experimental litters per group ($AP_{15\rightarrow15}$ CTIP2 and TBR1), 3 experimental litters per group ($AP_{12\rightarrow12}$), 3 experimental litters per group ($AP_{15\rightarrow12}$ CUX1 and TBR1) and 4 experimental litters ($AP_{15\rightarrow12}$ CTIP2). **d**, $AP_{15\rightarrow12}$ daughter neurons extend subcerebral projections via the internal capsule. Photomicrographs show RFP^+ axons from the same pup for each condition. Left, the laminar position of neurons in the corresponding pup. Experiments were repeated three times with similar results. CC, corpus callosum; IC, internal capsule. Scale bar, 15 μm. NS, not significant, $^*P < 0.05$, $^{**}P < 0.01$.

re-activation of this pathway within $AP_{15\rightarrow12}$ suggests a role in the respecification process. Together, these results reveal that resurgence of past neurogenic competences in $AP_{15\rightarrow12}$ is accompanied by a corresponding temporal rewind of their molecular identity.

We next examined whether this AP_{12}-like molecular respecification of $AP_{15\rightarrow12}$ also entailed a re-assignment of their functional features. For this purpose, we measured three key temporally regulated physiological parameters of these cells: their resting membrane potential, neurogenic mode and progeny clone size (Fig. 3a, e–g). We first addressed membrane potential, as progression of AP neurogenic competence is regulated by a progressive hyperpolarization of the resting membrane potential[25] (V_m). Consistent with a reassignment of AP neurogenic competence, $AP_{15\rightarrow12}$ V_m values were reset to those of APs in their E12.5 host, as was expression of V_m-regulating potassium channels transcripts (Fig. 3e, Extended Data Fig. 5e). Next, we examined neurogenic divisions, as symmetric divisions predominate early in corticogenesis, whereas asymmetric, neuron-generating divisions increase at later embryonic stages[26]. Accordingly, RFP^+SOX2^+ cells (that is, cycling transplanted APs) and $RFP^+NEUROD2^+$ cells (that is, their daughter neurons) were reassigned to E12 values in $AP_{15\rightarrow12}$ (Fig. 3f). Finally, we addressed clone size. The number of daughter neurons produced by a single AP decreases from around eight progeny at E12.5 (ref. [4]) to around three progeny at E14.5 (ref. [27]). Consistent with a temporally dynamic change in AP proliferation, mean oligoclone size increased in $AP_{15\rightarrow12}$ to values normally found in $AP_{12\rightarrow12}$ (Fig. 3g). Together, these three functional readouts reveal a wholesale rejuvenation of the molecular and physiological properties of $AP_{15\rightarrow12}$, which are reassigned to those of their younger host.

Of note, in contrast to $AP_{15\rightarrow12}$, AP_{12} transplanted into older hosts ($AP_{12\rightarrow15}$) were not respecified by their new niche in terms of membrane potential, neurogenic divisions, clone size or neurogenic competence (Extended Data Figs. 6, 7, Supplementary Note 3). The selective lack of temporal fate plasticity of $AP_{12\rightarrow15}$ is consistent with a shorter fate-decision-making G1 phase[28–30] and the comparatively weaker environment-sensing transcriptional programs of AP_{12} compared with AP_{15}[8]. Early-born APs are thus less sensitive to changes in their environment, potentially providing for robust early stages of corticogenesis in the mouse (Supplementary Discussion).

Late-born IPs lack temporal plasticity

Our results contrast with earlier findings in which ferret progenitor cells transplanted into younger hosts could no longer generate DL

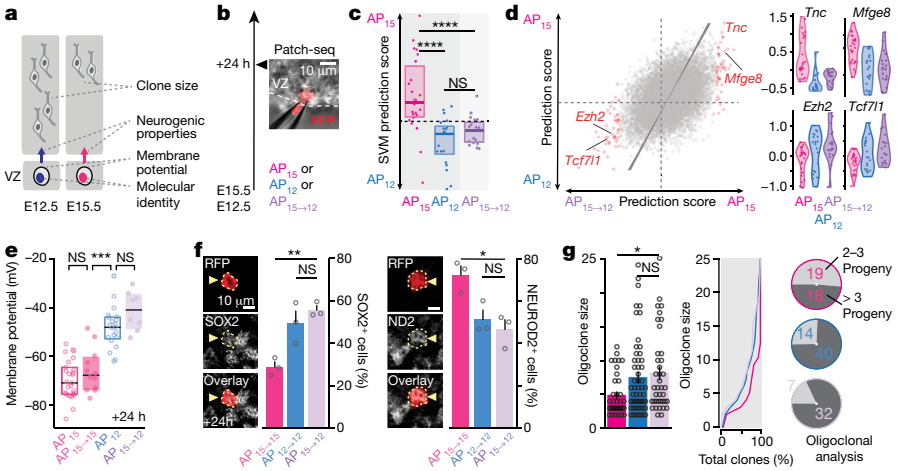

Fig. 3 | AP_{15} are respecified to AP_{12} upon heterochronic transplantation. a, Progenitor features used for analysis of $AP_{15\rightarrow12}$ identity. **b**, Summary of the experimental approach used for Patch-seq single-cell RNA sequencing. The image shows a patched RFP^+ AP. **c**, Support vector machine (SVM) classification reveals that $AP_{15\rightarrow12}$ acquire an AP_{12}-type molecular identity. Box plots in **c** and **e** show median and interquartile range. Two-tailed Kolmogorov–Smirnov test. **d**, $AP_{15\rightarrow12}$ repress AP_{15}-enriched transcripts and induce AP_{12}-enriched transcripts. Right, genes re-induced in $AP_{15\rightarrow12}$ include the Wnt-pathway regulator *Tcf7l1* and the PRC2 methyltransferase *Ezh2*. In **c**, **d**, $n = 20$ cells (AP_{12}), 26 cells (AP_{15}) and 19 cells ($AP_{15\rightarrow12}$). **e**, The membrane potential of $AP_{15\rightarrow12}$ depolarizes to AP_{12} values. Box plots indicate median and interquartile range. $n = 27$ cells (AP_{15}), 12 cells ($AP_{15\rightarrow15}$), 21 cells (AP_{12}) and 8 cells ($AP_{15\rightarrow12}$). Kruskal–Wallis test with post hoc Dunn's test. **f**, Neurogenic divisions decrease to AP_{12} values in $AP_{15\rightarrow12}$. $n = 3$ experimental litters per group. One-way ANOVA with post hoc Tukey test. **g**, The oligoclone size and the fraction of clones containing more than three progeny in $AP_{15\rightarrow12}$ increase to AP_{12} values. $n = 37$ oligoclones ($AP_{15\rightarrow15}$), 54 oligoclones ($AP_{12\rightarrow12}$) and 39 oligoclones ($AP_{15\rightarrow12}$). Kruskal–Wallis test with post hoc Dunn's test. **f**, **g**, Values are shown as mean ± s.e.m. SOX2, AP marker. NS, not significant, $^*P < 0.05$, $^{**}P < 0.01$, $^{***}P < 0.001$, $^{****}P < 0.0001$.

neurons[12,13]. In these seminal experiments, progenitors were identified by incorporation of radiolabelled thymidine, which labels S-phase cells across the ventricular zone (VZ), subventricular zone (SVZ) and outer SVZ[12,13]. Late in corticogenesis, and particularly in gyrencephalic species, the majority of progenitors are IP-type cells[31]. In these studies, the fate plasticity identified here may have been occluded by the overwhelming predominance of other, potentially less-plastic types of progenitor cell, and particularly by IP-type cells. In addition, in contrast to APs (which divide multiple times), IPs are thought to divide only once or twice before reaching a terminal division[7,9], potentially biasing radiolabelled thymidine-based quantifications towards the latter lineage.

To investigate the possibility of progenitor-type-specific differences in fate plasticity, we first reproduced the strategy used to isolate progenitors in these earlier experiments: following microdissection and dissociation of the dorsal pallium at E15.5, we used the thymidine analogue EdU to single-pulse-label VZ and SVZ progenitors and identify their progeny in the host. Following transplantation into E12.5 hosts, daughter neurons (identified as EdU^+ cells) were mostly located in SL, replicating earlier findings in the ferret (Extended Data Fig. 8a–c, Supplementary Table 1). Thus, our new results reflect cell-type rather than species-specific features of progenitor plasticity, and suggest that the competence for progenitor respecification is dependent on cell subtype.

In light of these results, we hypothesized that, whereas AP_{15} are temporally plastic, IP_{15} are committed to generating SL neurons. To test this possibility, we performed FlashTag labelling at E15.5 and waited 10 h before collection to allow daughter IPs to differentiate[14,15]. By this stage, more than 75% of $FlashTag^+$ cells had differentiated into IPs, as revealed by co-expression of TBR2 and the proliferation marker KI67[25] (Fig. 4a, Extended Data Fig. 8d). In contrast to $AP_{15\rightarrow12}$, $IP_{15\rightarrow12}$ essentially gave rise to SL neurons (Fig. 4b–d, Extended Data Fig. 8e, Supplementary Table 1). Accordingly, $IP_{15\rightarrow12}$ clone size was smaller than for $AP_{15\rightarrow12}$, consistent with fewer self-replicating divisions[4,7] (Extended Data Fig. 8f). Consistent with their location, $IP_{15\rightarrow12}$ daughter neurons expressed CUX1 but not CTIP2 (Extended Data Fig. 8g). These results demonstrate that—in contrast to AP_{15}—IP_{15} are committed progenitors with a fixed neurogenic competence.

Dynamic Wnt signalling drives $AP_{15\rightarrow12}$ respecification

Canonical Wnt signalling regulates AP neurogenic competence during corticogenesis[24,25] and Wnt transcripts (and particularly *Wnt7b*) are expressed in an early–high to late–low gradient in the developing neocortex (Extended Data Fig. 9a, b). Wnt-related transcriptional programs are induced in $AP_{15\rightarrow12}$ (Fig. 3d) and AP_{15} still express Wnt-receptor-related transcriptional programs (Extended Data Fig. 9c), suggesting that high levels of Wnt in the E12 niche may drive the neurogenic respecification of $AP_{15\rightarrow12}$. To test this possibility, we isolated AP_{15} in vitro and examined the fate of their daughter neurons in response to pharmacological activation of Wnt signalling or exposure to E12.5 cortex (Fig. 5a). As previously reported[8], the in vitro neurogenic competences of AP_{12} and AP_{15} remained distinct when using the transcription factor CTIP2 (a core determinant of DL neuron identity[1]) as a marker of normally early-born neurons (Fig. 5b, left). Activation of Wnt signalling with the GSK-3β inhibitor CHIR99021[32] in AP_{15} led to an increase in CTIP2-expressing daughter neurons to levels normally observed in AP_{12}, suggesting re-induction of earlier neurogenic programs (Fig. 5b, centre). Co-culturing AP_{15} with dissociated E12.5 cortex also re-induced the production of normally earlier-born daughter neurons; this plasticity was abolished when Wnt signalling was repressed by expressing the dominant negative form of TCF4 (DN-TCF4)[24,25] (Fig. 5b, right), strongly suggesting that the release of Wnt by the early cortex is a critical driving force for $AP_{15\rightarrow12}$ fate plasticity. Confirming this possibility, in vivo repression of canonical Wnt signalling in $AP_{15\rightarrow12}$ with an inducible DN-TCF4 construct prevented fate respecification, as these cells essentially gave rise to SL neurons (as AP_{15} normally do) (Fig. 5c). Together, these findings identify Wnt signalling as a core molecular pathway underlying $AP_{15\rightarrow12}$ fate plasticity.

Discussion

Our findings reveal that APs can revert their temporal identity and re-enter past molecular states to once again generate normally earlier-born neurons. By contrast, late-born IPs are committed progenitors that lack such fate plasticity. These results highlight an unexpected cell-type-specific diversity in the temporal plasticity of neocortical progenitors and reveal that AP fate progression occurs without detectable fate restriction during the neurogenic period

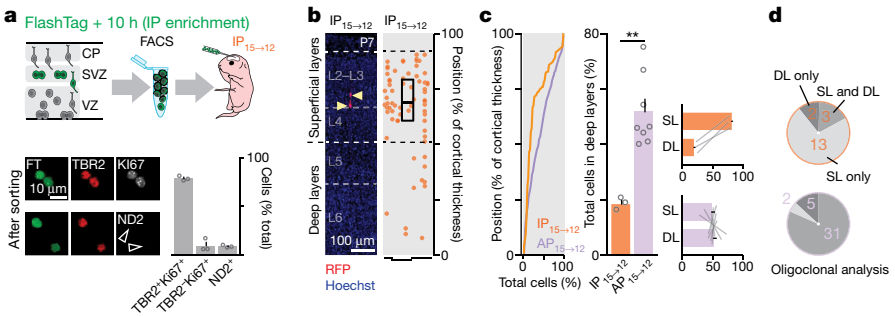

Fig. 4 | E15.5 IPs are committed to generating SL neurons. a, Schematic of the IP isolation and transplantation procedure. Values are shown as mean ± s.e.m.; $n = 3$ coverslips per group. **b**, E15.5 IPs transplanted into an E12.5 host ($IP_{15\rightarrow12}$) give rise to SL neurons. Each circle represents one cell, vertically aligned by single integration sites. Dashes delineate individual experimental litters. Box plot indicates median and interquartile range. **c**, Left, radial distribution of the daughter neurons of $IP_{15\rightarrow12}$ and $AP_{15\rightarrow12}$ at P7. Centre, fraction of daughter neurons in DL at P7. Two-tailed *t*-test. Right, modal distribution of daughter neurons in SL versus DL in the $IP_{15\rightarrow12}$ and $AP_{15\rightarrow12}$ conditions. Data are mean ± s.e.m.; $n = 3$ experimental litters ($IP_{15\rightarrow12}$) and 8 experimental litters ($AP_{15\rightarrow12}$). **d**, Oligoclonal integration-site analysis of the laminar distribution of daughter neurons. $AP_{15\rightarrow12}$ data in **c** and **d** have been reproduced from Fig. 1e–g for direct comparison with $IP_{15\rightarrow12}$. $^{**}P < 0.01$.

of corticogenesis. Thus, although the arc of development in whole organisms inescapably extends towards maturity, subsets of cells can be untethered from this course and remain able to re-enter past developmental states.

Although technical limitations precluded access to the cell-type-specific temporal plasticity identified here, the ability of progenitor cells to at least partially revert to earlier neurogenic states has been described in other settings[33–35]. For example, in the nervous system, late re-expression of early temporal identity factors in *Drosophila* neuroblasts leads to the production of previously generated cells[33]; late re-expression of the early cortical neuron transcription factor *Fezf2* leads to re-emergence of neurons with deep-layer identities[34]; inactivation of the transcription factor *Foxg1* leads to resurgence of early-born Cajal–Retzius neurons[35]; and AP depolarization gives rise to normally earlier-born neurons[25]. Thus, the transcriptional programs used during development remain amenable, in principle, to re-recruitment for some time after progenitor fate has progressed.

Our results reveal that activation of Wnt signalling is essential for $AP_{15\rightarrow12}$ fate plasticity to occur. Given that the neurogenic sequence is seemingly unaffected in $AP_{12\rightarrow15}$ despite lower environmental Wnt levels, Wnt signalling probably has a permissive role in the initiation of a temporal transcriptional program rather than an instructive role in the implementation of sequential steps of this program. In the developing *Xenopus* retina, Wnt signalling regulates progenitor fate transitions via induction of the PRC2 subunit *Ezh2*[23]. In APs—in which PRC2 controls fate progression—*Ezh2* is temporally regulated along an early–high to late–low gradient[8], and is also re-induced in $AP_{15\rightarrow12}$, such that evolutionarily conserved epigenetic regulation mechanisms may be involved. Although Wnt signalling appears to have a central role in the respecification process, the synergetic action of other

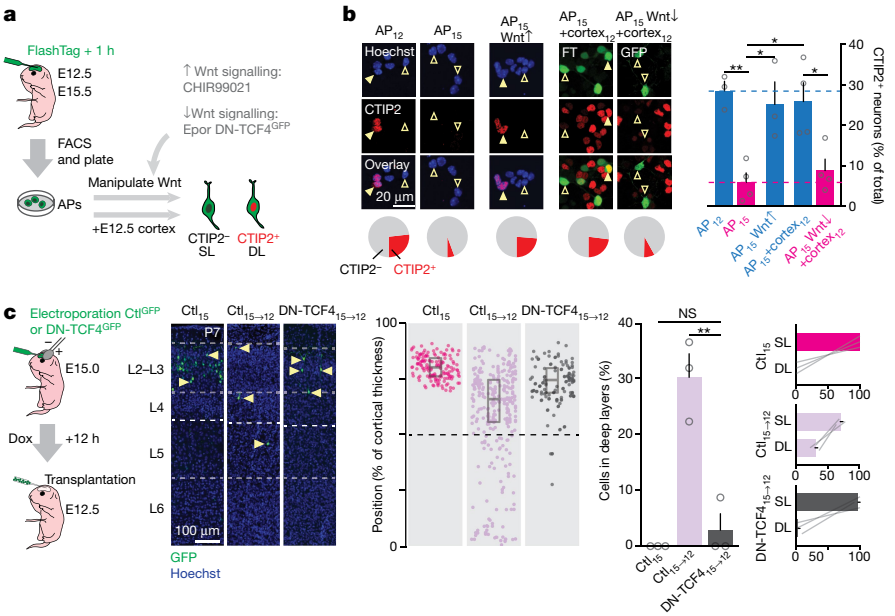

Fig. 5 | E12.5 cortex drives $AP_{15\rightarrow12}$ respecification through Wnt-pathway activation. a, Summary of the experimental approach. **b**, Over-activation (↑, using CHIR99021) and downregulation (↓, using DN-TCF4) of canonical Wnt signalling in AP_{15} and co-culture of AP_{15} with dissociated E12.5 cortex restores the generation of normally early-born, $CTIP2^+$ neurons. This E12.5 cortex effect is dependent on Wnt signalling. Data are mean ± s.e.m.; $n = 3$ coverslips per group (AP_{12}, AP_{15} Wnt↑), 4 coverslips per group (AP_{15}, AP_{15} + $cortex_{12}$, AP_{15}Wnt↓ + $cortex_{12}$). One-way ANOVA with post hoc Tukey test. **c**, In vivo blockade of canonical Wnt signalling by overexpression of DN-TCF4 blocks temporal respecification of $AP_{15\rightarrow12}$. Centre, radial distribution of daughter neurons at P7. Each circle represents one cell. Box plot indicates median and interquartile range. The two graphs on the right show the fraction of daughter neurons in deep layers at P7. Dox, doxycycline. Ctl, control. Data are mean ± s.e.m.; $n = 3$ experimental litters per group. One-way ANOVA with post hoc Tukey test. NS, not significant, $^{*}P < 0.05$, $^{**}P < 0.01$.

temporally dynamic environmental factors such as cell–cell interactions (for example, Notch signalling)[5,24,36], metabolic state[37] and feedback from nearby axons or newborn neurons (for example, via Sip1)[38,39] probably also contribute to the overall respecification process. It will therefore be important to understand the precise sequence of extrinsic, intrinsic, permissive and instructive events underlying such a notable level of plasticity, and to attempt to harness these processes for neuroregenerative purposes.

Online content

Any methods, additional references, Nature Research reporting summaries, source data, extended data, supplementary information, acknowledgements, peer review information; details of author contributions and competing interests; and statements of data and code availability are available at https://doi.org/10.1038/s41586-019-1515-6.

Received: 28 November 2018; Accepted: 29 July 2019;
Published online 28 August 2019.

1. Greig, L. C., Woodworth, M. B., Galazo, M. J., Padmanabhan, H. & Macklis, J. D. Molecular logic of neocortical projection neuron specification, development and diversity. *Nat. Rev. Neurosci.* **14**, 755–769 (2013).
2. Jabaudon, D. Fate and freedom in developing neocortical circuits. *Nat. Commun.* **8**, 16042 (2017).
3. Gaspard, N. et al. An intrinsic mechanism of corticogenesis from embryonic stem cells. *Nature* **455**, 351–357 (2008).
4. Gao, P. et al. Deterministic progenitor behavior and unitary production of neurons in the neocortex. *Cell* **159**, 775–788 (2014).
5. Okamoto, M. et al. Cell-cycle-independent transitions in temporal identity of mammalian neural progenitor cells. *Nat. Commun.* **7**, 11349 (2016).
6. Yuzwa, S. A. et al. Developmental emergence of adult neural stem cells as revealed by single-cell transcriptional profiling. *Cell Rep.* **21**, 3970–3986 (2017).
7. Mihalas, A. B. & Hevner, R. F. Clonal analysis reveals laminar fate multipotency and daughter cell apoptosis of mouse cortical intermediate progenitors. *Development* **145**, dev164335 (2018).
8. Telley, L. et al. Temporal patterning of apical progenitors and their daughter neurons in the developing neocortex. *Science* **364**, eaav2522 (2019).
9. Mihalas, A. B. et al. Intermediate progenitor cohorts differentially generate cortical layers and require Tbr2 for timely acquisition of neuronal subtype identity. *Cell Rep.* **16**, 92–105 (2016).
10. Vasistha, N. A. et al. Cortical and clonal contribution of Tbr2 expressing progenitors in the developing mouse brain. *Cereb. Cortex* **25**, 3290–3302 (2015).
11. Kowalczyk, T. et al. Intermediate neuronal progenitors (basal progenitors) produce pyramidal-projection neurons for all layers of cerebral cortex. *Cerebral Cortex* **19**, 2439–2450 (2009).
12. Frantz, G. D. & McConnell, S. K. Restriction of late cerebral cortical progenitors to an upper-layer fate. *Neuron* **17**, 55–61 (1996).
13. Desai, A. R. & McConnell, S. K. Progressive restriction in fate potential by neural progenitors during cerebral cortical development. *Development* **127**, 2863–2872 (2000).
14. Telley, L. et al. Sequential transcriptional waves direct the differentiation of newborn neurons in the mouse neocortex. *Science* **351**, 1443–1446 (2016).
15. Govindan, S., Oberst, P. & Jabaudon, D. *In vivo* pulse labeling of isochronic cohorts of cells in the central nervous system using FlashTag. *Nat. Protoc.* **13**, 2297–2311 (2018).
16. Nagashima, F. et al. Novel and robust transplantation reveals the acquisition of polarized processes by cortical cells derived from mouse and human pluripotent stem cells. *Stem Cells Dev.* **23**, 2129–2142 (2014).
17. Fishell, G. Striatal precursors adopt cortical identities in response to local cues. *Development* **121**, 803–812 (1995).
18. Brüstle, O., Maskos, U. & McKay, R. D. Host-guided migration allows targeted introduction of neurons into the embryonic brain. *Neuron* **15**, 1275–1285 (1995).
19. Cadwell, C. R. et al. Electrophysiological, transcriptomic and morphologic profiling of single neurons using Patch-seq. *Nat. Biotechnol.* **34**, 199–203 (2016).
20. Fuzik, J. et al. Integration of electrophysiological recordings with single-cell RNA-seq data identifies neuronal subtypes. *Nat. Biotechnol.* **34**, 175–183 (2016).
21. Kuwahara, A. et al. Tcf3 represses Wnt-β-catenin signaling and maintains neural stem cell population during neocortical development. *PLoS ONE* **9**, e94408 (2014).
22. Pereira, J. D. et al. Ezh2, the histone methyltransferase of PRC2, regulates the balance between self-renewal and differentiation in the cerebral cortex. *Proc. Natl Acad. Sci. USA* **107**, 15957–15962 (2010).
23. Aldiri, I., Moore, K. B., Hutcheson, D. A., Zhang, J. & Vetter, M. L. Polycomb repressive complex PRC2 regulates *Xenopus* retina development downstream of Wnt/β-catenin signaling. *Development* **140**, 2867–2878 (2013).
24. Mutch, C. A., Funatsu, N., Monuki, E. S. & Chenn, A. β-catenin signaling levels in progenitors influence the laminar cell fates of projection neurons. *J. Neurosci.* **29**, 13710–13719 (2009).
25. Vitali, I. et al. Progenitor Hyperpolarization Regulates the Sequential Generation of Neuronal Subtypes in the Developing Neocortex. *Cell* **174**, 1264–1276 (2018).
26. Haubensak, W., Attardo, A., Denk, W. & Huttner, W. B. Neurons arise in the basal neuroepithelium of the early mammalian telencephalon: a major site of neurogenesis. *Proc. Natl Acad. Sci. USA* **101**, 3196–3201 (2004).
27. Llorca, A. et al. Heterogeneous progenitor cell behaviors underlie the assembly of neocortical cytoarchitecture. Preprint at https://www.biorxiv.org/content/10.1101/494088v1 (2018).
28. Soufi, A. & Dalton, S. Cycling through developmental decisions: how cell cycle dynamics control pluripotency, differentiation and reprogramming. *Development* **143**, 4301–4311 (2016).
29. Sela, Y., Molotski, N., Golan, S., Itskovitz-Eldor, J. & Soen, Y. Human embryonic stem cells exhibit increased propensity to differentiate during the G1 phase prior to phosphorylation of retinoblastoma protein. *Stem Cells* **30**, 1097–1108 (2012).
30. Takahashi, T., Nowakowski, R. S. & Caviness, V. S. Jr. The cell cycle of the pseudostratified ventricular epithelium of the embryonic murine cerebral wall. *J. Neurosci.* **15**, 6046–6057 (1995).
31. Reillo, I. & Borrell, V. Germinal zones in the developing cerebral cortex of ferret: ontogeny, cell cycle kinetics, and diversity of progenitors. *Cereb. Cortex* **22**, 2039–2054 (2012).
32. Naujok, O., Lentes, J., Diekmann, U., Davenport, C. & Lenzen, S. Cytotoxicity and activation of the Wnt/beta-catenin pathway in mouse embryonic stem cells treated with four GSK3 inhibitors. *BMC Res. Notes* **7**, 273 (2014).
33. Kohwi, M., Lupton, J. R., Lai, S.-L., Miller, M. R. & Doe, C. Q. Developmentally regulated subnuclear genome reorganization restricts neural progenitor competence in *Drosophila*. *Cell* **152**, 97–108 (2013).
34. Molyneaux, B. J., Arlotta, P., Hirata, T., Hibi, M. & Macklis, J. D. Fezl is required for the birth and specification of corticospinal motor neurons. *Neuron* **47**, 817–831 (2005).
35. Hanashima, C., Li, S. C., Shen, L., Lai, E. & Fishell, G. *Foxg1* suppresses early cortical cell fate. *Science* **303**, 56–59 (2004).
36. Mizutani, K., Yoon, K., Dang, L., Tokunaga, A. & Gaiano, N. Differential Notch signalling distinguishes neural stem cells from intermediate progenitors. *Nature* **449**, 351–355 (2007).
37. Knobloch, M. et al. A fatty acid oxidation-dependent metabolic shift regulates adult neural stem cell activity. *Cell Rep.* **20**, 2144–2155 (2017).
38. Toma, K., Kumamoto, T. & Hanashima, C. The timing of upper-layer neurogenesis is conferred by sequential derepression and negative feedback from deep-layer neurons. *J. Neurosci.* **34**, 13259–13276 (2014).
39. Seuntjens, E. et al. Sip1 regulates sequential fate decisions by feedback signaling from postmitotic neurons to progenitors. *Nat. Neurosci.* **12**, 1373–1380 (2009).

METHODS

Mice. Experiments were performed using CD1 (Charles River) and CAG::mRFP1 (B6.Cg-Tg(CAG-mRFP1)1F1Hadj/J, JAX 005884)[40] mice. CAG::mRFP1 mice were bred on a CD1 background for at least ten generations before use. E0.5 was established as the day of vaginal plug. Both female and male embryos were used throughout the study. All experimental procedures were approved by the Geneva Cantonal Veterinary Authorities, Switzerland.

In utero FlashTag labelling. FlashTag injections were performed at E12.5, E15.5 and E17.5 as previously described[14,15]. In brief, pregnant mice were anaesthetized with isoflurane and an abdominal incision was made to access the uterine horns. Half a microlitre of 10 mM carboxyfluorescein succinimidyl ester (CellTraceTM CFSE, Life Technologies, C34554) or CytoTell Blue (AAT Bioquest, 22251) (FlashTag) was injected into the lateral ventricles of embryos using a picospritzer. The abdominal wall was sutured and the embryos allowed to develop until collection.

Preparation of cell suspension and in utero cell transplantation. One hour after FlashTag labelling (unless otherwise stated), donor embryos were collected in ice-cold HBSS and the dorsal pallium was microdissected under stereomicroscopic guidance (Leica, M165 FC) using a microscalpel. Tissue from six to eight littermates was pooled and incubated in 400 μl TrypLE (Gibco, 12605-010) for 3 min at 37 °C. TrypLE was inactivated by adding HBSS containing 0.1% BSA and the tissue was mechanically dissociated by triturating with a 1-ml pipette. Cells were filtered through a 70-μm cell strainer, centrifuged (150 r.p.m., 5 min) and resuspended in fluorescence-activated cell sorting (FACS) buffer (L15 medium containing 2 mg ml^{-1} glucose, 0.1% BSA, 1:50 citrate phosphate dextrose, 10 units ml^{-1} DNase I and 1 μM $MgCl_2$). Cells were sorted on an S3e Cell Sorter (BioRad) or a BD FACS Aria II flow cytometer (BD Biosciences) and the top 5–10% brightest cells[14,15], were collected in ice-cold FACS buffer. Sorted cells were centrifuged (150 r.p.m., 5 min) and resuspended in HBSS containing 10 mM EGTA[16] and 0.1% fast green to a final density of 25,000–75,000 cells per microlitre. Cells were kept on ice until the start of the transplantation procedure. Five hundred nanolitres of the cell suspension (corresponding to approximately 12,500–37,500 cells) was injected into the lateral ventricles of each host embryo using a picospritzer.

Continuous EdU labelling. A 10 mg ml^{-1} EdU solution was prepared in (1:1) DMSO:water. An osmotic pump (Alzet, 1003D) was filled with the solution and pre-incubated at 37 °C for 4–12 h. The pump was placed in the peritoneal cavity of the dam at the end of the surgical procedure to allow for continuous administration of EdU. If continuous delivery was required for more than 3 days (that is, when started at E12.5), a new pump prepared in the same way as above was introduced after 72 h. Revelation of EdU was performed using Click-it chemistry following the manufacturer's instructions (Invitrogen, C10340, C10338, C10337).

Oligoclonal analysis. Integration sites were defined as sites containing transplanted cells that are separated from other transplanted cells by at least 500 μm in either direction. Cells within each integration site are likely to correspond to progeny of a few integrated cells (Extended Data Fig. 1b).

In utero electroporation and plasmids. In utero electroporations were performed as previously described[25]. In brief, a 1.5 μg $μl^{-1}$ DNA solution was prepared in sterile PBS containing 0.01 mg ml^{-1} fast green. Half a microlitre of DNA solution was injected unilaterally into the lateral ventricle of embryos using a picospritzer and electroporation was performed by applying 5 electric pulses (25 V for E12.5, 45 V for E15.0 and E15.5, 55 V for E17.5; 50 ms at 1 Hz) with a square-wave electroporator (Nepa Gene, Sonidel Limited). For piggyBac electroporations a DNA solution containing 1:2 transposon pPB-CAG-EmGFP and hyperactive piggyBac transposase (pRP-Puro-CAGG-Pbase) was used[41]. Other plasmids used in this study were pCAG-IRES-GFP, pCAG-IRES-tdTOM, pGR-dnTCF4-pGK-GFP[25], inducible DN-TCF construct: pCWX-pTF-dnTCF4-PGK-GFP-E2A-rtTA[42]; and Wnt reporter construct: pGR-M38-TOPdGFP (Addgene 17114) co-electroporated with pCAG-IRES-tdTomato. For activation of transgene expression from the inducible DN-TCF4 construct, drinking water supplemented with 1 mg ml^{-1} doxycycline (Sigma) was administered immediately after in utero electroporation for 12 h until collection of embryos, and for additional 12 h after transplantation of cells.

In vitro experiments. For the analyses of marker expression in $FlashTag^+$ cells sorted by FACS 1 h or 10 h after labelling (Figs 1a, 4a), sorted cells were resuspended in FACS buffer at a density of 250,000 cells per ml, seeded on glass coverslips coated with poly-D-lysine and laminin and maintained at 37 °C with 5% CO_2 for 30 min to allow cells to adhere to the coverslips, followed by processing for immunocytochemistry.

For AP_{15} and AP_{12} experiments (Fig. 5c), $FlashTag^+$ cells, sorted by FACS from E15.5 or E12.5 embryos, were resuspended in culture medium (DMEM/F12 supplemented with 1% N2, 10 ng/ml FGF2, 1% penicillin–streptomycin (Gibco)) at a density of 250,000 cells per ml, seeded on glass coverslips coated with poly-D-lysine and laminin and maintained at 37 °C with 5% CO_2. For Wnt-pathway over-activation experiments, 5 μM of the GSK-3β inhibitor CHIR-99021[32] was added to the culture medium during plating of cells. For co-culture experiments, the cortex (that is, VZ, SVZ and CP) of wild-type E12.5 embryos was dissociated as described in 'Preparation of cell suspension and in utero cell transplantation' and co-cultured together with $FlashTag^+$ or GFP^+ FACS-sorted cells from E15.5 embryos at a density of 1,000,000 cells per ml (at a ratio of 1:4 of $FlashTag^+$ or GFP^+ cells and E12.5 cortex). In these co-cultures, AP_{15} daughter neurons were identified on the basis of fluorescence (they were generated from $FlashTag^+$ or GFP^+ mother cells). Cells were maintained for four days in vitro until processing for immunocytochemistry.

Immunohistochemistry. Embryonic brains were collected in PBS and fixed in 4% paraformaldehyde (PFA) overnight at 4 °C. Postnatal mice were perfused with 4% PFA and brains were post-fixed in 4% PFA overnight at 4 °C. Coronal sections 50–100 μm in thickness were cut using a vibrating microtome (Leica, VT100S). Antigen retrieval was performed by incubating the sections in citrate buffer solution (Dako, S1699) for 20 min at 82 °C. Sections were rinsed 3 times in PBS and incubated overnight at 4 °C with primary antibodies diluted in PBS containing 3% BSA and 0.3% Triton-X100. Sections were rinsed 3 times in PBS containing 0.1% Tween-20 (PBST) and incubated for 1 h at room temperature with corresponding secondary antibodies (1:500, Life Technologies). Sections were washed twice with PBST and incubated with Hoechst for 5 min (1:5,000 in PBS, Life Technologies, 33342) to stain nuclei. Sections were dry-mounted on slides using Fluoromount (Sigma, F4680).

Immunocytochemistry of FACS-sorted cells. Cells were fixed with 4% PFA (15 min at room temperature), rinsed 3 times with PBS and permeabilized by incubation with 0.25% Triton-X-100 in PBS for 10 min, followed by 3 washes in PBS. Blocking was performed with 1% BSA in PBST for 1 h, followed by incubation with primary antibodies overnight at 4 °C. Cells were rinsed 3 times in PBS and incubated for 1 h at room temperature with corresponding secondary antibodies (1:500, Life Technologies). Cells were then washed 2 times with PBS and incubated with Hoechst for 5 min (1:5,000 in PBS) to stain nuclei. Coverslips were mounted on slides using Fluoromount.

Antibodies. Rat anti-CTIP2 (1:500; Abcam, AB18465); rabbit anti-CUX1 (1:500; Santa Cruz; sc-13024); rabbit anti-dsRed (1:1,000; Clonetech; 632496); mouse anti-GFAP (1:500; Sigma, G3893); rabbit anti-KI67 (1:250; Abcam, AB15580); rabbit anti-NEUROD2 (1:1,000; Abcam, AB104430); rat anti-RFP (1:500; Chromotek; 5F8); goat anti-SOX2 (1:500; SC Biotech, SC17320); rabbit anti-SOX2 (1:500; Abcam, AB97959); mouse anti-SOX2 (1:500; Santa Cruz; sc-365823); rabbit anti-TBR1 (1:500; Abcam; AB31940); rabbit anti-TBR2 (1:500; Abcam; ab23345) and rat anti-TBR2 (1:500; Invitrogen, 14-4875-82) were used.

Electrophysiology and collection of cells for single-cell RNA sequencing. Three-hundred-micrometre-thick coronal slices were prepared 24 h after transplantation or FlashTag labelling. Slices were kept for at least 30 min in artificial cerebrospinal fluid (aCSF) at 33 °C (125 mM NaCl, 2.5 mM KCl, 1 mM $MgCl_2$, 2.5 mM $CaCl_2$, 1.25 mM NaH_2PO_4, 26 mM $NaHCO_3$ and 11 mM glucose, saturated with 95% O_2 and 5% CO_2) before recording. The slices were then transferred in the recording chamber, submerged and continuously perfused with aCSF. The internal solution used for the experiments contained 140 mM potassium methansulfonate, 2 mM $MgCl_2$, 4 mM NaCl 0.2 mM EGTA, 10 mM HEPES, 3 mM Na_2ATP, 0.33 mM GTP and 5 mM creatine phosphate (pH 7.2, 295 mOsm).

For resting membrane-potential recordings, immediately after the whole-cell configuration, resting membrane potential was measured in current-clamp mode. Membrane potential was monitored every 10 s and averaged for 6 consecutive acquisitions, within the first 2 min after the whole-cell configuration establishment. V_m remained stable within conditions and was significantly different across conditions throughout the duration of the recording, indicating that V_m recordings are not influenced by cytoplasmic dilution with the patch pipette solution. Recordings were amplified (Multiclamp 700, Axon Instruments), filtered at 5 kHz and digitalized at 20 kHz (National Instrument Board PCI-MIO-16E4, IGOR WaveMetrics), and stored on a personal computer for further analyses (IGOR PRO WaveMetrics). Values are represented as mean ± s.e.m.

For collection of cells for patch single-cell RNA sequencing, FlashTag-labelled non-transplanted or RFP^+-transplanted progenitors located in the ventricular zone were patched with a patch pipette containing 1 μl of internal solution supplemented with 1 U $μl^{-1}$ RNase inhibitor (Takara). To facilitate the aspiration of the cell, low pipette resistance was used (4–3 MΩ). Once in whole-cell configuration, a slit depression was applied to the pipette to aspirate the intracellular content. The complete aspiration of the cell was observed under high magnification (Nikon Eclipse FN1, 60× lens) as retraction of the cytoplasm and total aspiration of the nucleus. The patch pipette was then slowly retracted and the pipette tip containing the cell content was broken into a PCR RNase free Eppendorf containing 8 μl of lysis buffer from the SMART-Seq v4 3′ DE Kit and stored at −80 °C until further processing.

Single-cell RNA sequencing. cDNA synthesis and preamplification were performed using the SMART-Seq v4 3′ DE Kit following the manufacturer's instructions (Takara). Single-cell RNA-sequencing libraries of the cDNA were prepared using the Nextera XT DNA library prep kit (Illumina). Libraries were

multiplexed and sequenced according to the manufacturer's recommendations with paired-end reads using the HiSeq4000 plat-form (Illumina) with an expected depth of one million reads per single cell, and a final mapping read length of 50 bp. Each pool contained cells from different collection days and conditions. All single-cell RNA capture and sequencing experiments were performed at the Genomics Core Facility of the University of Geneva. The sequenced reads were aligned to the mouse genome (GRCm38) using STAR aligner. The number of reads per transcript was calculated with the open-source HTSeq Python library. All analyses were computed on the Vital-It cluster administered by the Swiss Institute of Bioinformatics.

Single-cell RNA sequencing analysis. *Cell filtering*. A total of 91 cells (AP_{12}: 31 cells; AP_{15}: 31 cells; $AP_{15\rightarrow12}$: 29 cells) were sequenced. Cells expressing <2,000 genes or >12% of mitochondrial genes were excluded ($n = 26$ cells). A total of 65 cells were analysed (AP_{12}: 20 cells; AP_{15}: 26 cells; $AP_{15\rightarrow12}$: 19 cells). Gene expression was normalized to reads per million and log-transformed. Cell-cycle effect was corrected for using the ccRemover package. We used the SVM method implemented in the bmrm R package to classify the age of progenitors with genes showing minimal expression (10,407), as previously described[43]. The model was trained with a subset of AP_{12} and AP_{15} progenitors and the 30 most-weighted genes were used for leave-one-out cross-validation of additional AP_{12} and AP_{15} progenitors and prediction of $AP_{15\rightarrow12}$ cells. The same method was applied to build a model to classify AP_{15} and $AP_{15\rightarrow12}$, selecting for 100 most-weighted genes. The datasets generated in this study are available in the GEO repository under accession number GSE122644.

Wnt-related gene expression analysis. For Extended Data Fig. 9a, a publicly available dataset[8] containing 831 APs (FlashTag + 1h) and 923 young neurons (FlashTag + 24h) from E12 to E15 FlashTag injections (E12: 189 APs, 268 neurons; E13: 207 APs, 223 neurons; E14: 134 APs, 219 neurons; E15: 301 APs, 213 neurons) was used to extract *Wnt*-transcript expression profiles across developmental stages.

For Extended Data Fig. 9b, the expression landscapes of *Wnt* transcripts were taken from the online resource http://genebrowser.unige.ch/telagirdon[8].

For Extended Data Fig. 9c, *Wnt* receptor-related expression data in AP_{15} and AP_{12} were extracted from ref. [8] (E12: 189 APs; E15: 301 APs).

Image acquisition, quantification and statistical analyses. Images were acquired using an Eclipse 90i epifluorescence microscope (Nikon), a LSM 700 linescan confocal (Carl Zeiss) or a Nikon A1r spectral line-scan confocal (Nikon) and analysed with ImageJ software. For analysis of transplantations, brains from each recipient litter (that is, containing cells from one independent FACS experiment per donor litter) were pooled for analysis and considered as one replicate (n), except when indicated otherwise. Sample size was not determined in advance, but was based on consistency of results between litters and between pups within a given litter; a sample size of 3–5 litters was considered sufficient. Experiments under different conditions were performed on different days on the basis of mouse availability. Blinding was used for data collection and analysis of pharmacological treatments in in vitro experiments, but not performed in other experiments owing to the unambiguous nature of measurements and systematic analyses used in these experiments. Only neurons located in the neocortex were included in analysis, and glia were excluded based on morphology unless otherwise stated. For analysis of the radial position of cells, the cortical thickness was defined as the area between pia and subplate (comprising L1–L6). All results are shown as mean ± s.e.m., except where indicated otherwise. Boxplots indicate the median and interquartile range. The following convention was used: $*P < 0.05$, $**P < 0.01$, $***P < 0.001$ and $****P < 0.0001$.

For Figs. 1a, 4a, three to four coverslips (n) from two independent FACS experiments were analysed for each condition. For Fig. 1a, 73 cells were stained for SOX2 and ND2 (% $SOX2^+$: 98.91 ± 1.09; % $ND2^+$: 1.09 ± 1.09); 50 cells were stained for TBR2 (% $TBR2^+$: 0). For Fig. 4a, 121 cells were stained for TBR2 and KI67 (% $TBR2^+$ $KI67^+$: 78.84 ± 1.41; % $TBR2^-$ $KI67^+$: 9.21 ± 3.37); 214 cells were stained for ND2 (% $ND2^+$: 8.4 ± 0.75).

For Fig. 1b–g, cells from all transplantation experiments collected at P7 were included in the analysis. $AP_{15\rightarrow15}$: 180 cells from 8 experimental litters (n) and 37 integration sites; $AP_{12\rightarrow12}$: 401 cells from 6 experimental litters and 54 integration sites; $AP_{15\rightarrow12}$: 316 cells from 8 experimental litters and 39 integration sites. For Fig. 1b–d, the radial position of cells within the neocortex was measured and normalized to the cortical thickness. The normalized radial position for each cell was plotted and cells were aligned on the x axis per integration site. Chronic EdU labelling was used to identify transplanted host-born neurons in all experiments, except donor litters: $AP_{15\rightarrow15}$ 1, 2, 7, 8; $AP_{12\rightarrow12}$ 2, 3, 5; $AP_{15\rightarrow12}$ 1, 3, 4, 5. For Fig. 1e, density and cumulative distribution plots were used to additionally display the radial positions of cells. For Fig. 1f, left, the percentage of total cells in DL per donor litter is plotted ($AP_{15\rightarrow15}$: 5.0 ± 2.05; $AP_{12\rightarrow12}$: 50.5 ± 7.07; $AP_{15\rightarrow12}$: 51.62 ± 4.53). A one-way ANOVA with post hoc Tukey test was used. Right, the percentage of total cells in DL and SL per donor litter is plotted. SL and DL values from the same experiment are connected with lines. For Fig. 1g, individual integration sites were examined for each condition and the number of oligoclones containing cells in only SL, only DL or both SL and DL were plotted.

For Fig. 2, a subset of cells depicted in Fig. 1 was analysed for molecular marker expression. The normalized radial position of labelled and non-labelled cells and the total percentage of cells expressing the respective marker were plotted. $AP_{15\rightarrow15}$: 42 cells from 4 experimental litters were stained for CUX1 (% $CUX1^+$: 94.1 ± 3.42); 54 cells from 3 experimental litters were stained for CTIP2 (% $CTIP2^+$: 1.28 ± 1.28); 48 cells from 3 experimental litters were stained for TBR1 (% $TBR1^+$: 0). $AP_{12\rightarrow12}$: 102 cells from 3 experimental litters were stained for CUX1 (% $CUX1^+$: 57.19 ± 4.69); 53 cells from 3 experimental litters were stained for CTIP2 (% $CTIP2^+$: 28.13 ± 3.52); 55 cells from 3 experimental litters were stained for TBR1 (% $TBR1^+$: 31.11 ± 2.94). $AP_{15\rightarrow12}$: 59 cells from 3 experimental litters were stained for CUX1 (% $CUX1^+$: 52.82 ± 9.76); 81 cells from 4 experimental litters were stained for CTIP2 (% $CTIP2^+$: 29.34 ± 7.43); 38 cells from 3 experimental litters were stained for TBR1 (%$TBR1^+$: 22.13 ± 4.18). A one-way ANOVA with post hoc Tukey test was used.

For Fig. 2d, the corpus callosum and the internal capsule of host mice containing at least 30 RFP^+ neurons in the neocortex were imaged using a LSM 700 line scan confocal (Carl Zeiss) equipped with a 40× oil-immersion objective and analysed for the presence or absence of RFP^+ fibres. For generation of photomicrographs depicted in the figure, the LUT of the image was set to grey values and inverted using ImageJ software for better visualization of RFP^+ fibres.

For Fig.3c and Extended Data Fig. 7a, $n = AP_{12}$: 20 cells, AP_{15}: 26 cells, $AP_{15\rightarrow12}$: 19 cells. For Fig. 3c, a two-tailed Kolmogorov–Smirnov test was used.

For Fig. 3e and Extended Data Fig. 8b, the resting membrane potential of cells located in the VZ was recorded 24 h after transplantation or FlashTag labelling. AP_{15}: −70.58 ± 1.51 mV, $n = 27$ cells. $AP_{15\rightarrow15}$: −66.8 ± 2.58 mV, 12 cells. AP_{12}: −48.96 ± 1.82 mV, 21 cells. $AP_{15\rightarrow12}$: −42.08 ± 2.82 mV, 8 cells. $AP_{12\rightarrow15}$: −55.19 ± 2.91 mV; 12 cells. A Kruskal–Wallis test with a post hoc Dunn's test was used.

For Fig. 3f, left, $AP_{15\rightarrow15}$: 56 cells from 3 experimental litters (n) were stained for SOX2 (% $SOX2^+$: 28.97 ± 2.41); 54 cells from 3 experimental litters were stained for ND2 (% $ND2^+$: 72.59 ± 3.88). $AP_{12\rightarrow12}$: 49 cells from 3 experimental litters were stained for SOX2 (% $SOX2^+$: 49.75 ± 5.57); 72 cells from 3 experimental litters were stained for ND2 (% $ND2^+$: 51.24 ± 4.38). $AP_{15\rightarrow12}$: 134 cells from 3 experimental litters were stained for SOX2 (% $SOX2^+$: 55.83 ± 1.97); 63 cells from 3 experimental litters were stained for ND2 (% $ND2^+$: 46.56 ± 4.57). Right, for analysis of cells remaining in the VZ 24h after transplantation, cells from 3 experimental litters (n), including a subset of cells used for SOX2/ND2 expression analysis, were analysed. $AP_{15\rightarrow15}$: 120 cells total (% cells in VZ: 34.28 ± 4.13). $AP_{12\rightarrow12}$: 66 cells total (% cells in VZ: 56.6 ± 0.95). $AP_{15\rightarrow12}$: 134 cells total (% cells in VZ: 54.15 ± 3.94). A one-way ANOVA with post hoc Tukey test was used.

For Fig. 3g and Extended Data Fig. 6d, individual integration sites were examined for each condition and the number of cells per integration site (oligoclone size) and the fraction of integration sites containing 2–3 or >3 cells were plotted. Mean oligoclone size (cell number): $AP_{15\rightarrow15}$: 4.87 ± 0.5; $AP_{12\rightarrow12}$: 7.43 ± 0.8; $AP_{15\rightarrow12}$: 8.1 ± 0.9; $AP_{12\rightarrow15}$: 9.04 ± 0.99. $N = AP_{15\rightarrow15}$: 37 oligoclones; $AP_{12\rightarrow12}$: 54 oligoclones; $AP_{15\rightarrow12}$: 39 oligoclones and $AP_{12\rightarrow15}$: 78 oligoclones. A one-way ANOVA with post hoc Tukey test was used.

For Fig. 4b–d, 81 cells from 3 experimental litters (n) and 18 integration sites were analysed. For comparison, $AP_{15\rightarrow12}$ data reproduced from Fig. 1f are shown. For Fig. 4d, the normalized radial position of RFP^+ EdU^+ cells was plotted and cells were aligned on the x axis per integration site. For Fig. 4c, left, density and cumulative distribution plots were used to additionally display the radial positions of cells. Centre, the percentage of total cells in DL per donor litter is plotted ($IP_{15\rightarrow12}$: 18.98 ± 1.27). A Student's t-test was used. Right, the percentage of total cells in DL and SL per donor litter is plotted. SL and DL values from the same experiment are connected with lines. For Fig. 4d, individual integration sites were examined for each condition and the number of oligoclones containing cells in only SL, only DL or both SL and DL were plotted.

For Fig. 5b, three to four coverslips (n) from at least two independent FACS experiments were analysed for each condition. Per cent $CTIP2^+$ of $FlashTag^+$ or GFP^+ daughter neurons: AP_{15}: 5.59 ± 5.21; AP_{12}: 26.78 ± 2.26; AP_{15} Wnt↑: 23.7 ± 5.22; AP_{15} + $cortex_{12}$: 24.4 ± 4.34; $AP_{15\,DN\text{-}TCF4}$ + $cortex_{12}$: 8.34 ± 2.63. A one-way ANOVA with post-hoc Tukey test was used.

For Fig. 5c, the normalized radial position of GFP^+ cells is plotted. Right, the percentage of total cells in DL per n is plotted (Ctl_{15}: 0; $Ctl_{15\rightarrow12}$: 30.11 ± 4.16; $DN\text{-}TCF4_{15\rightarrow12}$: 2.9 ± 2.9). Far right, the percentage of total cells in DL and SL per donor litter is plotted. SL and DL values from the same experiment are connected with lines.

For Extended Data Fig. 1b, the number of cells per integration site was analysed 6 h after transplantation of $AP_{15\rightarrow15}$. A total of 93 cells from 3 independent experiments (n), corresponding to 43 integration sites, were analysed. Number of cells per integration site: 1–6 (mean: 2.16; median: 2).

For Extended Data Fig. 1d, brains were collected at consecutive time points after $AP_{15\rightarrow15}$ transplantation or E15.5 FlashTag labelling. The distance of cells to the lateral ventricle was measured using ImageJ. RFP: 6 h: 46 cells, 14.89 ± 1.99 μm; 12 h: 21 cells, 29.54 ± 7.35; 24 h: 30 cells, 68.95 ± 13.25; 48 h: 30 cells, 259.4 ± 26.85; 72 h: 31 cells, 636.2 ± 63.42. FlashTag: 6 h: 36 cells, 35.29 ± 3.78; 12 h: 25 cells, 69.9 ± 5.27; 24 h: 33 cells, 92.79 ± 8.36; 48 h: 39 cells, 225.3 ± 23.97; 72 h: 31 cells, 681.2 ± 36.43.

For Extended Data Figs 2a, b, 3a, 7, 8c, e, images from all cells used for analysis are shown for each condition. In the plots, the normalized radial position is shown. Cells are aligned on the *x* axis per integration site. For Extended Data Figs 2, 3, 5, 9, EdU labelling was used to identify transplanted host-born neurons in all experiments, except: $AP_{15\rightarrow15}$: donor litters 1, 2, 7, 8; $AP_{12\rightarrow12}$: donor litters 2, 3, 5; $AP_{15\rightarrow12}$: donor litters 1, 3, 4, 5, $AP_{12\rightarrow15}$: donor litters 2, 3, 6. For Extended Data Fig. 8c, only EdU^+ cells were included in analysis.

For Extended Data Fig. 2c, d, the radial position of GFP^+ or RFP^+ neurons within the neocortex was normalized to the cortical thickness. For GFP^+ cells, at least three pups (*n*), and three sections from different rostro-caudal levels per pup, were used per condition. The layer position for each cell was plotted. In cortical areas with no anatomically distinguishable L4, the lowest 1/3 of L2/3 was arbitrarily considered as L4. Cells in L2/3 (%): $Epor_{PB15}$: 92.13 ± 1; $Epor_{PB12}$: 38.83 ± 1.28; $AP_{15\rightarrow15}$: 85.79 ± 2.58; $AP_{12\rightarrow12}$: 41.33 ± 5.75. Cells in L4 (%): $Epor_{PB15}$: 7.39 ± 0.66; $Epor_{PB12}$: 13.67 ± 1.24; $AP_{15\rightarrow15}$: 10.78 ± 2.24; $AP_{12\rightarrow12}$: 8.13 ± 3.06. Cells in L5 (%): $Epor_{PB15}$: 0.34 ± 0.28; $Epor_{PB12}$: 22.46 ± 3.45; $AP_{15\rightarrow15}$: 5.6 ± 2.16; $AP_{12\rightarrow12}$: 25.68 ± 3.99. Cells in L6 (%): $Epor_{PB15}$: 0.14 ± 0.14; $Epor_{PB12}$: 28.26 ± 2.87; $AP_{15\rightarrow15}$: 1.01 ± 0.79; $AP_{12\rightarrow12}$: 24.86 ± 4.05. $AP_{15\rightarrow15}$ and $AP_{12\rightarrow12}$ distribution plots are copied from Fig. 1. A two-way ANOVA with post-hoc Tukey test was used.

For Extended Data Fig. 3b, the layer position for all cells depicted in Fig. 1 was plotted. Cells in L2–L3 (%): $AP_{15\rightarrow12}$: 43.16 ± 3.63. Cells in L4 (%); $AP_{15\rightarrow12}$: 5.75 ± 1.54. Cells in L5 (%): $AP_{15\rightarrow12}$: 33.09 ± 2.15. Cells in L6 (%): $AP_{15\rightarrow12}$: 18 ± 3.90. $AP_{15\rightarrow15}$ and $AP_{12\rightarrow12}$ data are re-plotted from Extended Data Fig. 2 for direct comparison with $AP_{15\rightarrow12}$. $N = AP_{15\rightarrow15}$: 7 experimental litters; $AP_{12\rightarrow12}$: 6 experimental litters; $AP_{15\rightarrow12}$: 8 experimental litters. A two-way ANOVA with post hoc Tukey test was used.

For Extended Data Fig. 3c, the total percentage of RFP^+ or GFP^+ glial cells is plotted. Glial cells were identified on the basis of morphology. This approach was confirmed by GFAP immunofluorescence. % glial cells: $AP_{17\rightarrow12}$: 91.48 ± 6.27; $Epor_{PB17}$: 97.65 ± 0.47. $n = 3$ experimental litters per group. Two-tailed *t*-test.

For Extended Data Fig. 4a–c, $AP_{15\rightarrow12}$ distribution plots and photomicrographs showing expression of CUX1, CTIP2 and TBR1 within the neocortical layers are copied from Fig. 2.

For Extended Data Fig. 4e, $n = N_{15\rightarrow12}$: 3 experimental litters; $AP_{15\rightarrow12}$: 8 experimental litters. $AP_{15\rightarrow12}$ data has been reproduced from Fig. 1f for direct comparison with $N_{15\rightarrow12}$.

For Extended Data Fig. 6c, $AP_{12\rightarrow15}$: % $SOX2^+$: 59.35 ± 2.18; % $ND2^+$: 41.36 ± 1.73. $AP_{12\rightarrow12}$ and $AP_{15\rightarrow15}$ data are reproduced from Fig. 3f for direct comparison with $AP_{12\rightarrow15}$. $n = 3$ experimental litters per group. A one-way ANOVA with post-hoc Tukey test was used.

For Extended Data Fig. 6e–g, $AP_{12\rightarrow15}$: % total $CTIP2^+$: 25.05 ± 2.54; % total $TBR1^+$: 31.89 ± 1.89; %; $CUX1^+$ neurons in DL: $AP_{12\rightarrow15}$: 71.21 ± 6.86; $AP_{12\rightarrow12}$: 15.06 ± 5.16. $AP_{12\rightarrow12}$ and $AP_{15\rightarrow15}$ data are reproduced from Fig. 2 for direct comparison with $AP_{12\rightarrow15}$. $n = 3$ experimental litters per group, except $AP_{12\rightarrow15}$ TBR1: 2 experimental litters. A one-way ANOVA with post hoc Tukey test was used.

For Extended Data Fig. 8b, 34 cells from 3 experimental litters (*n*) and 11 integration sites were analysed. Left, the normalized radial position of EdU^+ cells was plotted and cells were aligned on the *x* axis per integration site. Right, top, the layer position for each cell was plotted. SL and DL values from the same experiment are connected with lines. Right, bottom, individual integration sites were examined and the number of oligoclones containing cells in only SL, only DL or both SL and DL were plotted.

For Extended Data Fig. 8d, three sections from different rostro-caudal levels from three pups (*n*) were used to quantify the number of $FlashTag^+$ $TBR2^+$ $KI67^+$ cells 10 h after FlashTag labelling at E15.5 (%$FlashTag^+$ $TBR2^+$ $KI67^+$: 70.99 ± 2.81).

For Extended Data Fig. 8f, the number of cells per integration site (oligoclone size) was analysed pooling all cells from previous experiments. $AP_{15\rightarrow12}$ data are reproduced from Fig. 3g for direct comparison with $IP_{15\rightarrow12}$. $AP_{15\rightarrow12}$: 8.1 ± 0.9; $IP_{15\rightarrow12}$: 3.41 ± 0.54. $n = AP_{15\rightarrow12}$: 39 oligoclones; $IP_{15\rightarrow12}$: 17 oligoclones.

For Extended Data Fig. 8g, a subset of EdU^+ cells depicted in Fig. 4d–f was analysed for molecular marker expression. The normalized radial position of labelled and non-labelled cells and the total percentage of cells expressing the respective marker were plotted. A total of 15 cells from 2 experimental litters (*n*) were stained for CUX1 (% $CUX1^+$: 93.75 ± 6.25); 63 cells from 3 experimental litters (*n*) were stained for CTIP2 (% $CTIP2^+$: 0.83 ± 0.83).

Reporting summary. Further information on research design is available in the Nature Research Reporting Summary linked to this paper.

Data availability

The datasets generated in this study are available in the GEO repository under accession number GSE122644.

40. Long, J. Z., Lackan, C. S. & Hadjantonakis, A.-K. Genetic and spectrally distinct *in vivo* imaging: embryonic stem cells and mice with widespread expression of a monomeric red fluorescent protein. *BMC Biotechnol.* **5**, 20 (2005).
41. Chen, F. & LoTurco, J. A method for stable transgenesis of radial glia lineage in rat neocortex by piggyBac mediated transposition. *J. Neurosci. Methods* **207**, 172–180 (2012).
42. Bocchi, R. et al. Perturbed Wnt signaling leads to neuronal migration delay, altered interhemispheric connections and impaired social behavior. *Nat. Commun.* **8**, 1158 (2017).
43. Teo, C. H., Vishwanathan, S. V. N. & Smola, A. Bundle methods for regularized risk minimization. *J. Mach. Learn. Res.* **11**, 311–365 (2010).

Acknowledgements We thank members of the Jabaudon laboratory and E. Azim for comments on the manuscript. We thank O. Raineteau for providing plasmids. We thank A. S. Lopes, A. Benoit, the FACS facility, the Genomics Platform and the Bioimaging Facility of the University of Geneva for technical assistance. Work in the Jabaudon laboratory is supported by the Swiss National Science Foundation, the Fondation des HUG, and the Carigest Foundation. P.O. is supported by a fellowship from iGE3.

Author contributions P.O. and D.J. designed the experiments. P.O. performed the experiments with the help of C.C. and G.B.; S.F. performed the electrophysiology experiments and the collection of cells for Patch-seq with the help of P.O.; N.B. performed the bioinformatic analysis; P.O. and D.J. wrote the manuscript.

Competing interests : The authors declare no competing interests.

Additional information

Supplementary information is available for this paper at https://doi.org/10.1038/s41586-019-1515-6.

Correspondence and requests for materials should be addressed to D.J.

Peer review information *Nature* thanks André Goffinet and the other anonymous reviewer(s) for their contribution to the peer review of this work.

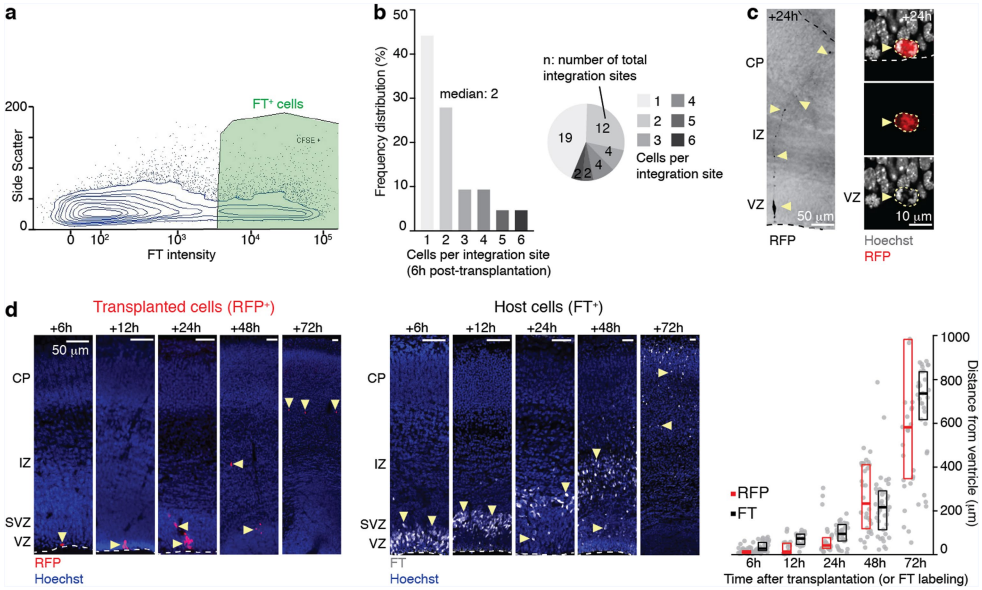

Extended Data Fig. 1 | Donor APs rapidly integrate the VZ and behave normally. a, FACS of FlashTag^{+} cells 1 h after labelling. **b**, Donor APs integrate the host VZ at discrete sites. Only a few APs (median = 2) are present at each site, such that daughter neurons found at single integration sites at P7 are probably born from a small number of initial APs (oligoclonal analysis, Figs. 1g, 4d, Extended Data Fig. 8b). **c**, Left, photomicrograph of a transplanted AP showing a radial glia morphology (maximum projection). Right, juxtaventricular mitosis in a transplanted AP. Experiments in **a**–**c** were repeated at least three times with similar results. **d**, The progeny of transplanted APs progressively migrate towards the cortical plate. The time course of this migration is similar to that of the host cells, as assessed by comparison with the migration of FlashTag-labelled endogenous cells. Box plots show median and interquartile range. $n = 46$ cells (RFP 6 h), 21 cells (RFP 12 h), 30 cells (RFP 24 h), 30 cells (RFP 48 h), 31 cells (RFP 72 h), 36 cells (FlashTag 6 h), 25 cells (FlashTag 12 h), 33 cells (FlashTag 24 h), 39 cells (FlashTag 48 h), 31 cells (FlashTag 72 h).

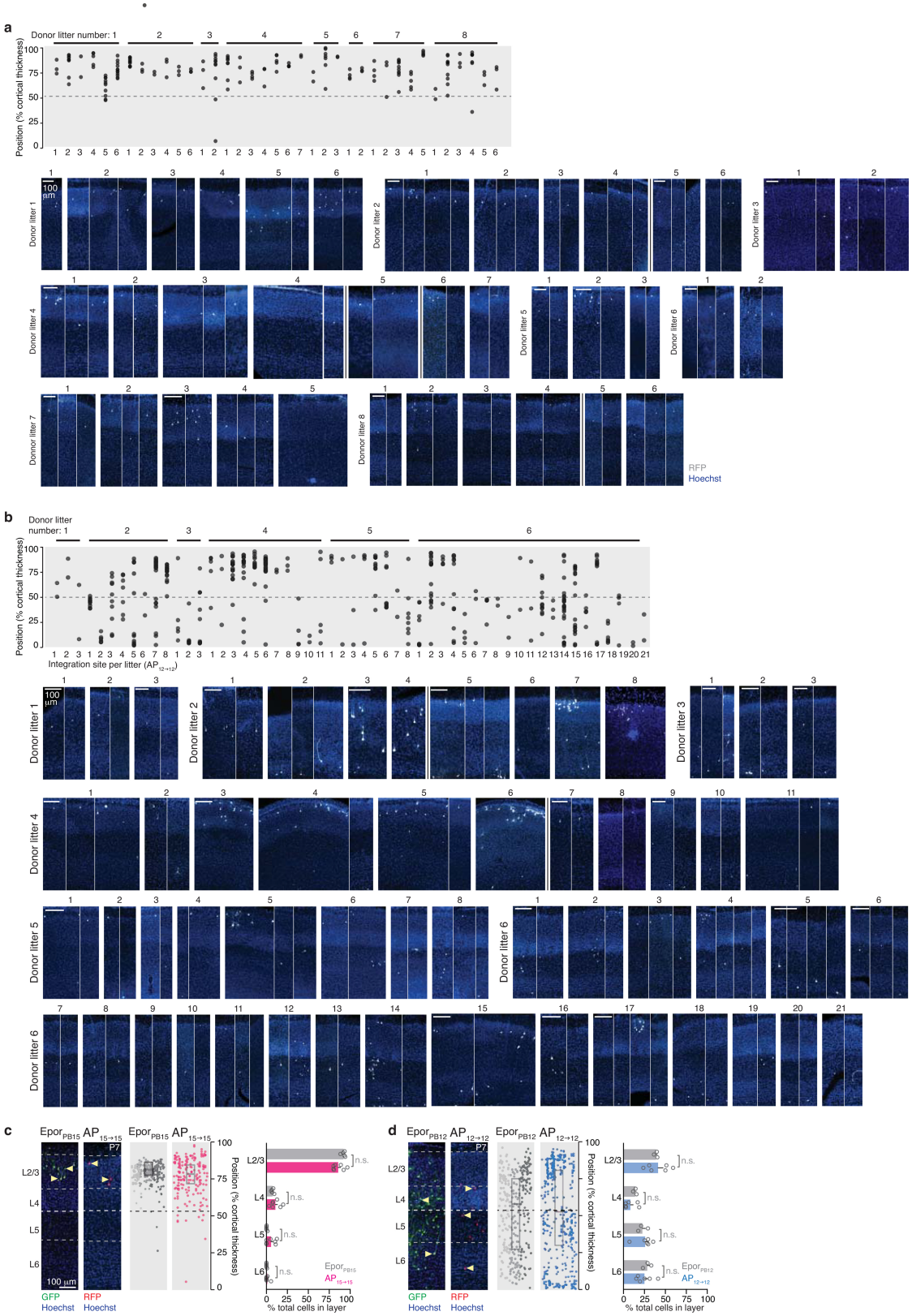

Extended Data Fig. 2 | See next page for caption.

Extended Data Fig. 2 | Analysis of single integration sites in $AP_{15\rightarrow15}$ and $AP_{12\rightarrow12}$—the transplantation procedure does not affect the neurogenic competence of APs. a, Isochronically transplanted E15.5 APs ($AP_{15\rightarrow15}$) essentially generate SL neurons. Photomicrographs: within each donor litter, illustrations are clustered by integration site. Where applicable, a vertical black line delineates distinct host pups within a given litter. Experiments were repeated eight times with similar results. **b**, Isochronically transplanted E12.5 APs ($AP_{12\rightarrow12}$) generate DL and SL neurons. Photomicrographs: within each donor litter, illustrations are clustered by integration site. Where applicable, a vertical black line delineates distinct host pups within a given litter. Experiments were repeated six times with similar results. **c**, The laminar distribution of daughter neurons in the $AP_{15\rightarrow15}$ condition is replicated by in utero electroporation of a piggyBac-transposon construct at E15.5, in the absence of transplantation. **d**, The laminar distribution of daughter neurons in the $AP_{12\rightarrow12}$ condition is replicated by in utero electroporation of a piggyBac-transposon construct at E12.5. c, d, Box plots show median and interquartile range. In bar graphs, values are shown as mean ± s.e.m.; $n = 5$ pups ($Epor_{PB15}$), 7 experimental litters ($AP_{15\rightarrow15}$), 3 pups ($Epor_{PB12}$), 6 experimental litters ($AP_{12\rightarrow12}$). Two-way ANOVA with post hoc Tukey test. Epor, in utero electroporation. $AP_{15\rightarrow15}$ and $AP_{12\rightarrow12}$ distribution plots are reproduced from Fig. 1.

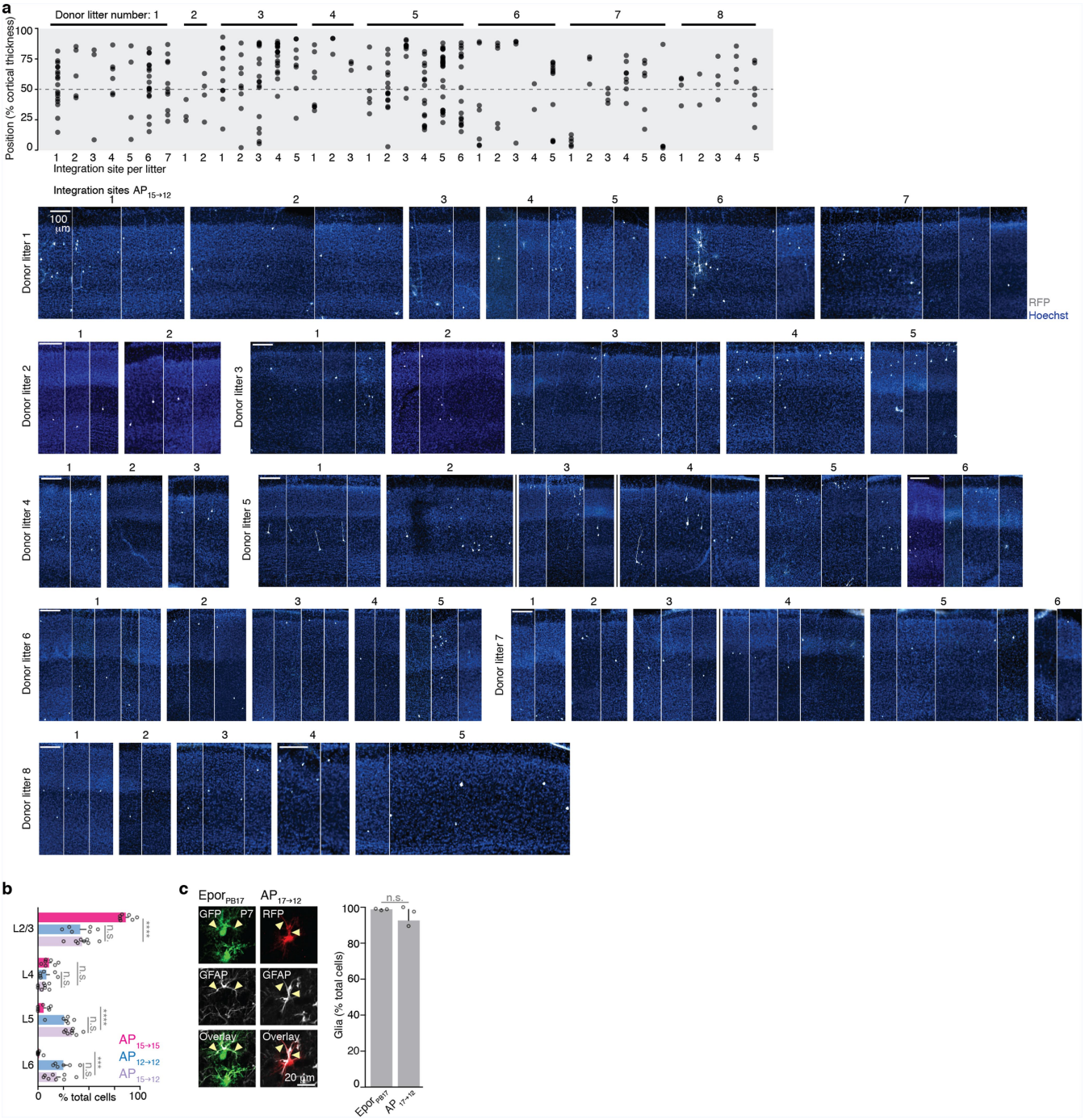

Extended Data Fig. 3 | Analysis of single integration sites in $AP_{15\rightarrow12}$ and lack of temporal respecification in gliogenic $AP_{17\rightarrow12}$. a, E15.5 APs transplanted into an E12.5 host ($AP_{15\rightarrow12}$) generate DL and SL neurons. Photomicrographs: within each donor litter, illustrations are clustered by integration site. Where applicable, a vertical black line delineates distinct host pups within a given litter. Experiments were repeated six times with similar results. **b**, Laminar distribution of daughter neurons across conditions. $AP_{15\rightarrow15}$ and $AP_{12\rightarrow12}$ distribution plots are reproduced from Extended Data Fig. 2 to enable direct comparison across conditions. Values are shown as mean ± s.e.m.; $n = 7$ experimental litters ($AP_{15\rightarrow15}$), 6 experimental litters ($AP_{12\rightarrow12}$), 8 experimental litters ($AP_{15\rightarrow12}$) . Two-way ANOVA with post hoc Tukey test. **c**, E17.5 APs transplanted into an E12.5 host ($AP_{17\rightarrow12}$) still almost exclusively generate glial cells. Arrowheads show examples of $GFAP^+$ cells. Values are shown as mean ± s.e.m.; $n = 3$ experimental litters per group. Two-tailed *t*-test. $^{***}P < 0.001$, $^{****}P < 0.0001$.

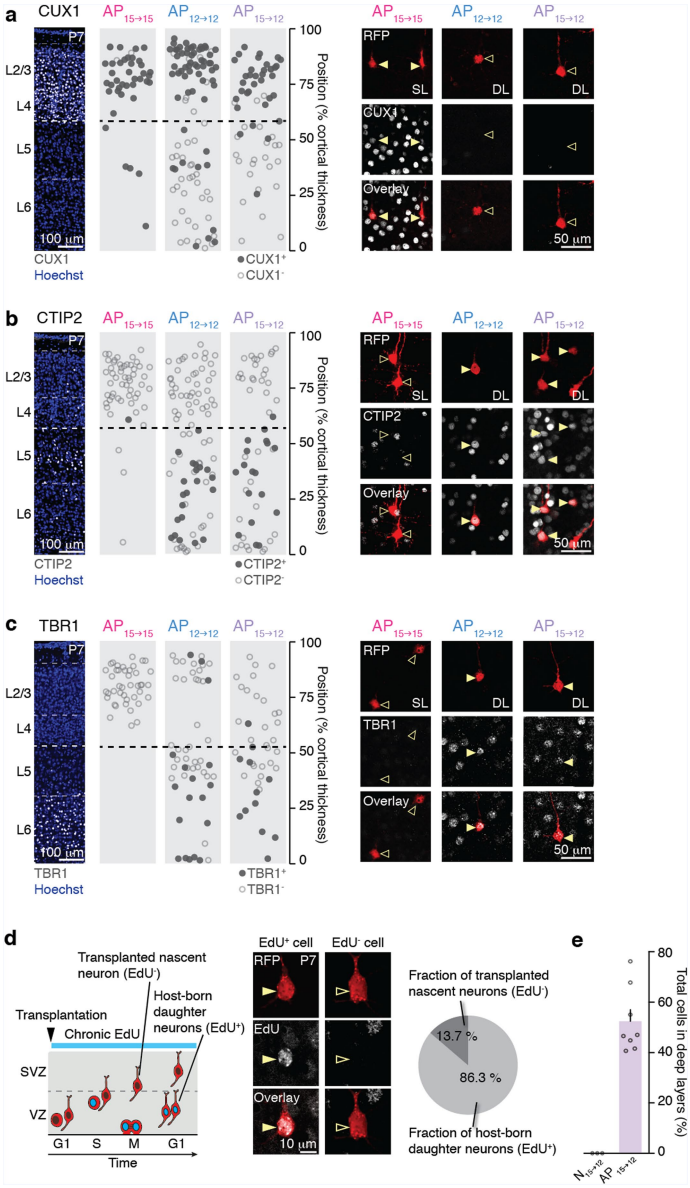

Extended Data Fig. 4 | Molecular markers of $AP_{15\rightarrow12}$ daughter neurons and approach used to identify transplanted nascent neurons. a, Reduced expression of the SL marker CUX1 in DL $AP_{15\rightarrow12}$ daughter neurons. **b**, Increased expression of the DL marker CTIP2 in DL $AP_{15\rightarrow12}$ daughter neurons. **c**, Increased expression of the DL marker TBR1 in DL $AP_{15\rightarrow12}$ daughter neurons. Photomicrographs showing pattern of expression of CUX1, CTIP2 and TBR1 are reproduced from Fig. 2. $AP_{15\rightarrow12}$ distribution plots in **a**–**c** have been reproduced from Fig. 2 for direct comparison. **d**, Left, schematic of the chronic EdU-labelling approach used to distinguish between nascent donor neurons and neurons born in the host. Centre, photomicrograph showing examples of an EdU^+ and an EdU^- donor neuron. Right, quantification of the fraction of EdU^- labelled neurons at P7 (that is, transplanted cells that never underwent division in the host). Experiments were repeated three times with similar results. **e**, Heterochronically transplanted E15.5 nascent neurons ($N_{15\rightarrow12}$) migrate to the superficial layers, as they would have done in their original host. Values are shown as mean ± s.e.m.; $n = 3$ experimental litters ($N_{15\rightarrow12}$), 8 experimental litters ($AP_{15\rightarrow12}$). $AP_{15\rightarrow12}$ data in **e** have been reproduced from Fig. 1f for direct comparison. M, mitosis; S, S phase.

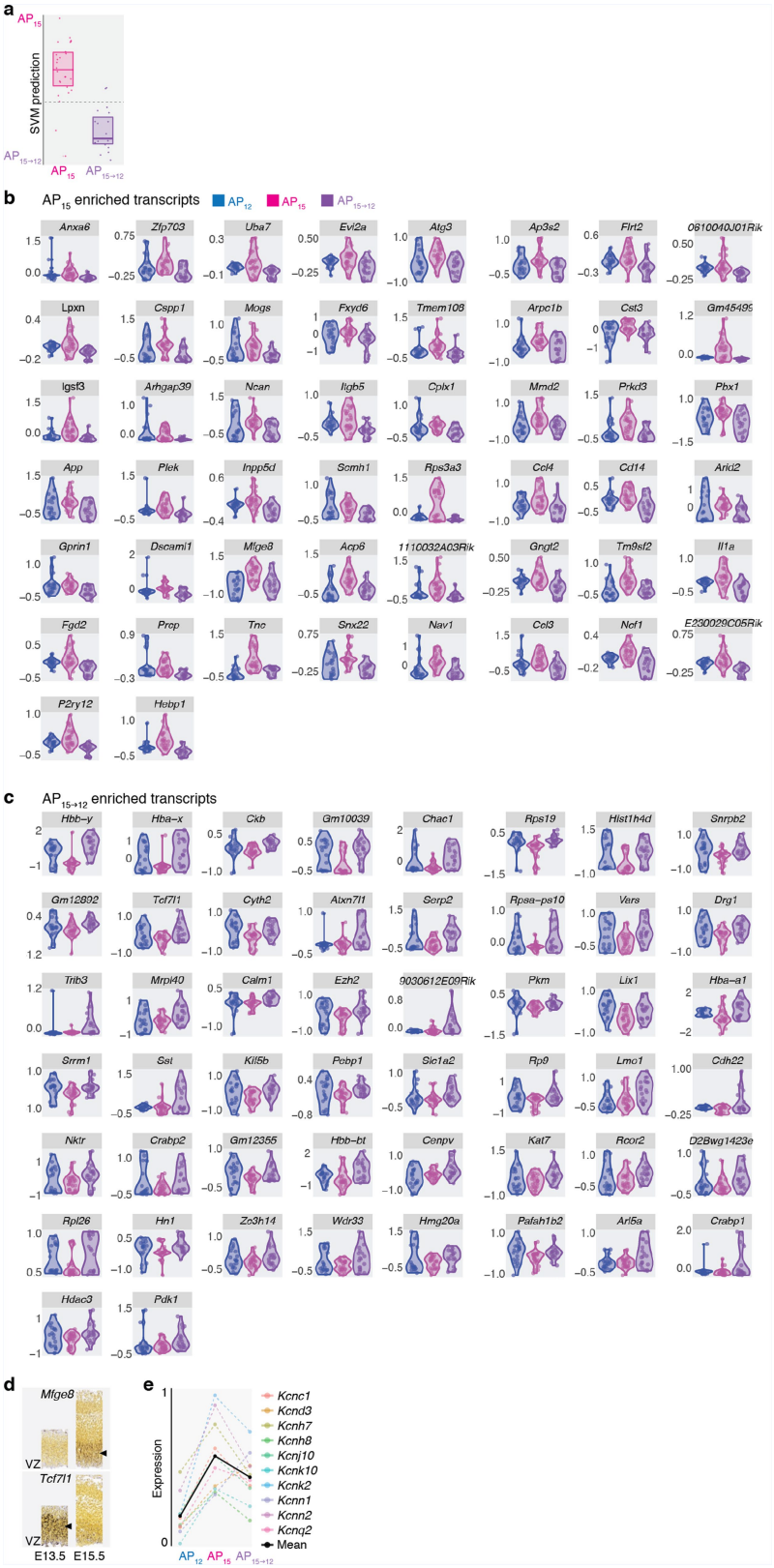

Extended Data Fig. 5 | Repression of AP_{15}-type transcriptional programs and re-induction of AP_{12}-type transcriptional programs in $AP_{15\rightarrow12}$. **a**, SVM classification of AP_{15} and $AP_{15\rightarrow12}$. Box plots indicate median and interquartile range. $n = 26$ cells (AP_{15}), 19 cells ($AP_{15\rightarrow12}$). **b**, Expression of the AP_{15} transcripts used in the model. **c**, Expression of the $AP_{15\rightarrow12}$ transcripts used in the model. In **b**, **c**, $n = 20$ cells (AP_{12}), 26 cells (AP_{15}), 19 cells ($AP_{15\rightarrow12}$). **d**, Examples of hybridizations from the Allen Developing Mouse Brain Atlas (© 2008 Allen Institute for Brain Science. Allen Developing Mouse Brain Atlas. Available from: http://developingmouse.brain-map.org/) corresponding to genes shown in Fig. 3d. **e**, The expression of potassium channels is repressed in $AP_{15\rightarrow12}$. $n = 20$ cells (AP_{12}), 26 cells (AP_{15}), 19 cells ($AP_{15\rightarrow12}$).

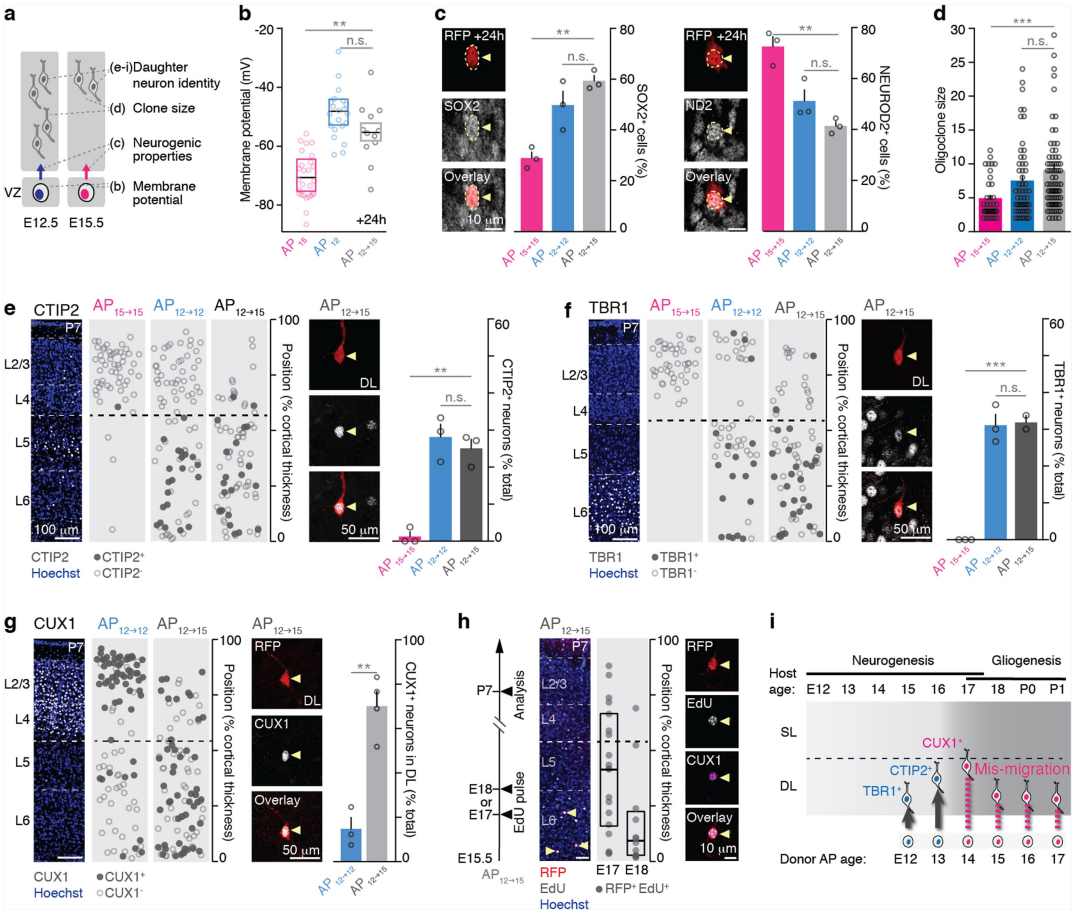

Extended Data Fig. 6 | Lack of temporal respecification of $AP_{12\rightarrow15}$. **a**, Parameters used to define $AP_{12\rightarrow15}$ identity. Letters refer to panels in this figure. **b**, The resting membrane potential of $AP_{12\rightarrow15}$ remains at AP_{12} values. Box plots indicate median and interquartile range; $n = 27$ cells (AP_{15}), 21 cells (AP_{12}), 12 cells ($AP_{12\rightarrow15}$). Kruskal–Wallis test with post hoc Dunn's test. **c**, Neurogenic divisions in $AP_{12\rightarrow15}$ remain at AP_{12} values. $n = 3$ experimental litters per group. One-way ANOVA with post hoc Tukey test. **d**, Number of cells per integration site at P7. Each point represents one oligoclone. The oligoclone size of $AP_{12\rightarrow15}$ remains at $AP_{12\rightarrow12}$ values. $n = 37$ oligoclones ($AP_{15\rightarrow15}$), 54 oligoclones ($AP_{12\rightarrow12}$), 78 oligoclones ($AP_{12\rightarrow15}$). Kruskal–Wallis test with post hoc Dunn's test. AP_{15}, AP_{12}, $AP_{12\rightarrow12}$ and $AP_{15\rightarrow15}$ data in **b**–**d** have been reproduced from Fig. 3 for direct comparison. **e**, $AP_{12\rightarrow15}$ still generate $CTIP2^+$ daughter neurons. $n = 3$ experimental litters per group. **f**, $AP_{12\rightarrow15}$ still generate $TBR1^+$ daughter neurons. $n = 3$ experimental litters ($AP_{15\rightarrow15}$ and $AP_{12\rightarrow12}$), 2 experimental litters ($AP_{12\rightarrow15}$). **g**, Mismigration of CUX1-expressing daughter neurons into DL in $AP_{12\rightarrow15}$. $n = 3$ experimental litters ($AP_{12\rightarrow12}$), 4 experimental litters ($AP_{12\rightarrow15}$). Photomicrographs showing pattern of expression of CUX1, CTIP2 and TBR2 are reproduced from Fig. 2. $AP_{12\rightarrow12}$ and $AP_{15\rightarrow15}$ data in **e**–**g** have been reproduced from Fig. 2 for direct comparison. Data in **c**–**g** are shown as mean ± s.e.m. One-way ANOVA with post hoc Tukey test (**e**–**g**). **h**, EdU pulse labelling at E17 and E18 shows progressive mismigration of increasingly later-born neurons in $AP_{12\rightarrow15}$. Box plots show mean and interquartile range. $n = 19$ cells (E17), 12 cells (E18). **i**, Summary of the mismigration phenotype in $AP_{12\rightarrow15}$. $^{**}P < 0.01$, $^{***}P < 0.001$.

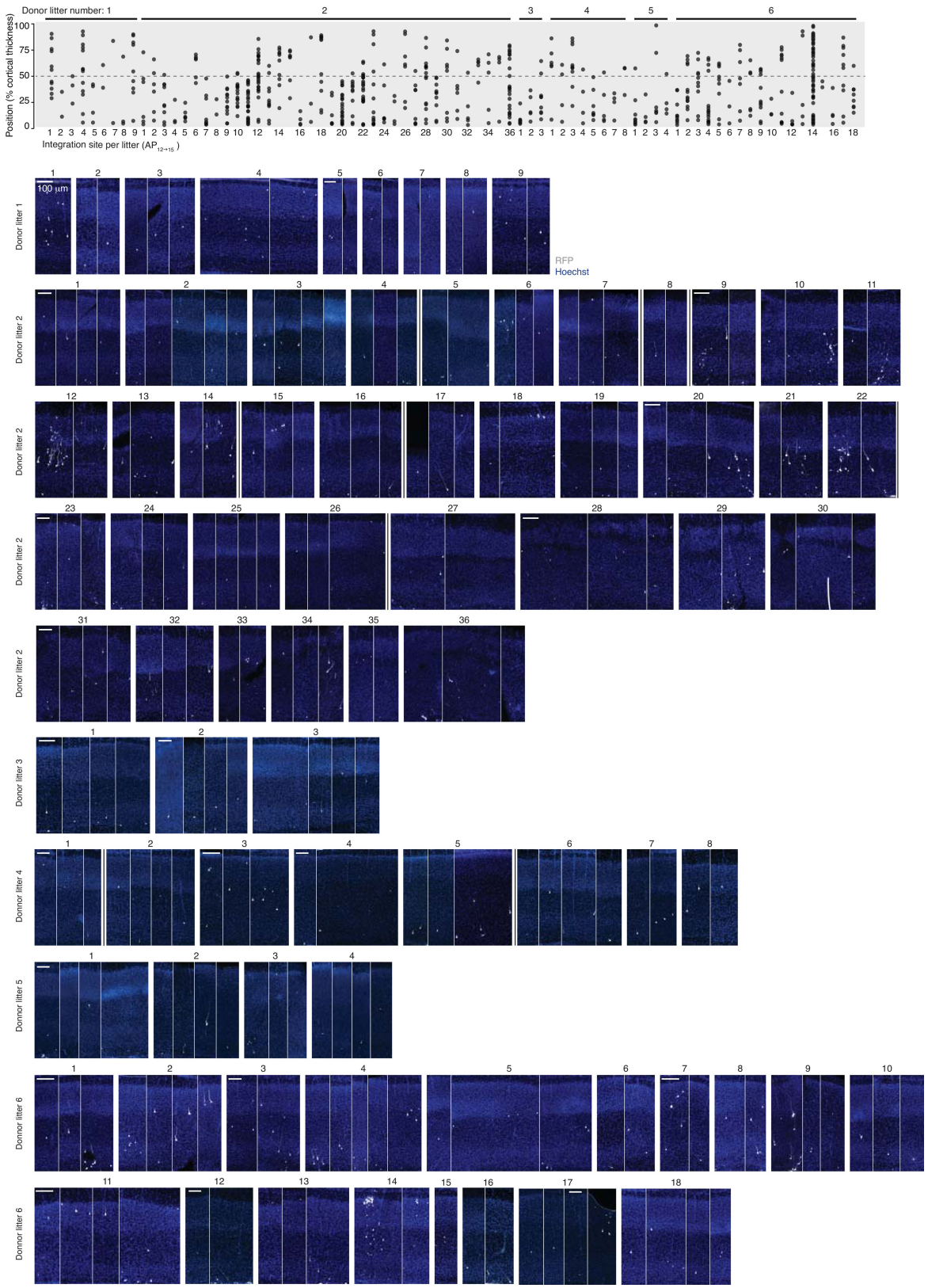

Extended Data Fig. 7 | Analysis of single integration sites in $AP_{12\rightarrow15}$. E12.5 APs transplanted into an E15.5 host ($AP_{12\rightarrow15}$) generate DL and SL neurons. Photomicrographs: within each donor litter, illustrations are clustered by integration site. Where applicable, a vertical black line delineates distinct host pups within a given litter. Experiments were repeated six times with similar results.

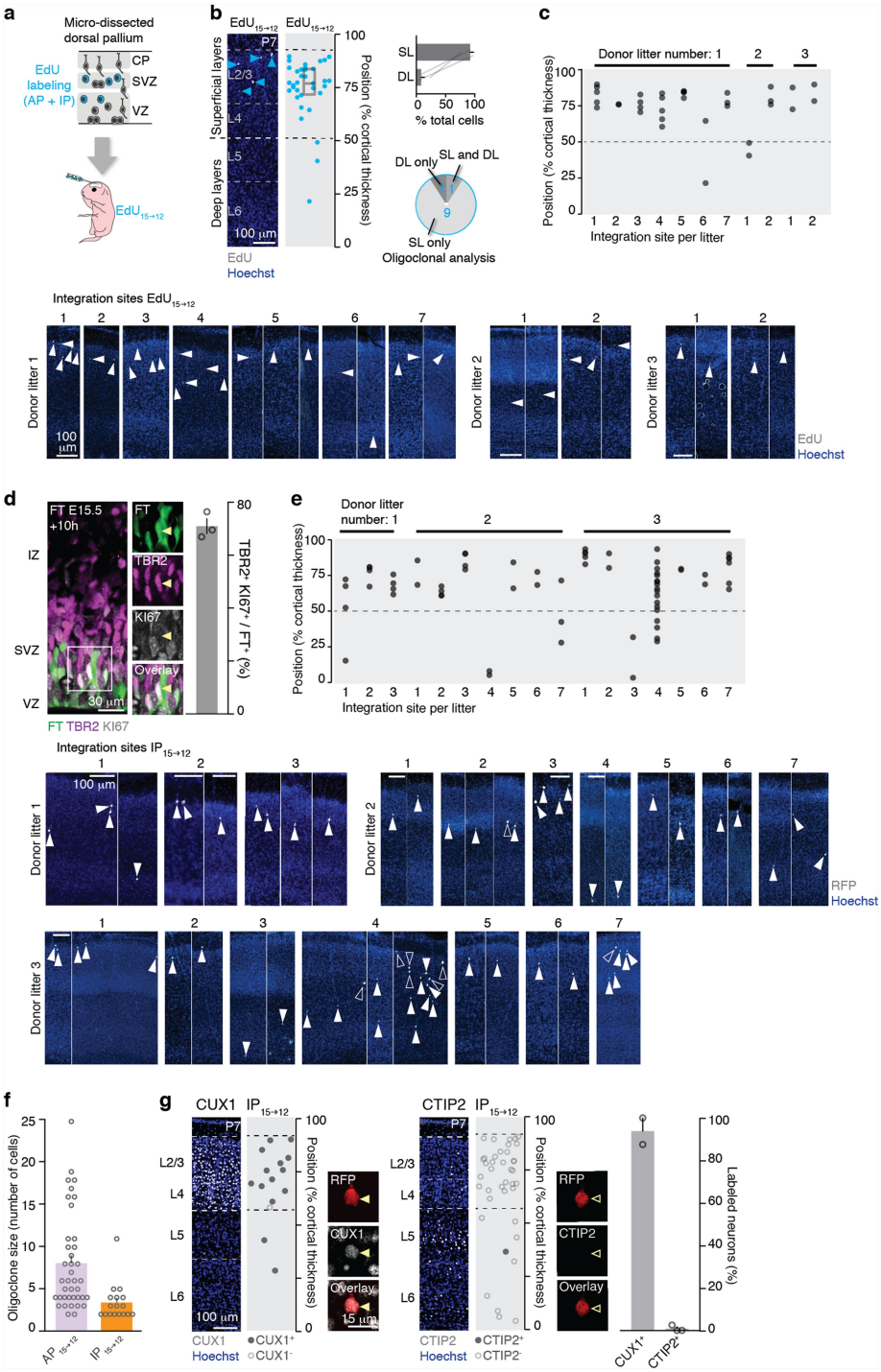

Extended Data Fig. 8 | Heterochronically transplanted IPs ($IP_{15\rightarrow12}$) generate SL neurons. a, Schematic showing EdU-based labelling and transplantation procedure. **b**, E15.5 EdU^+ cells transplanted into an E12.5 host ($EdU_{15\rightarrow12}$) still give rise to SL neurons (compare with Fig. 1d). Box plot shows median and interquartile range. Top right, modal distribution of daughter neurons in SL vs DL. Values are shown as mean ± s.e.m.; $n = 3$ experimental litters. Bottom right, laminar distribution of daughter neurons at single integration sites. Values refer to number of integration sites in each category. **c**, Heterochronically transplanted EdU-labelled progenitors ($EdU_{15\rightarrow12}$) essentially generate SL neurons. Photomicrographs: within each donor litter, illustrations are clustered by integration site. Experiments were repeated three times with similar results. **d**, Ten hours after FlashTag labelling, most cells have differentiated into IPs (that is, $KI67^+TBR2^+$ cells). Values are shown as mean ± s.e.m.; $n = 3$ pups. **e**, $IP_{15\rightarrow12}$ essentially give rise to SL neurons. Photomicrographs: within each donor litter, illustrations are clustered by integration site. Only EdU^+ neurons (filled arrowheads) were included in this analysis. Experiments were repeated three times with similar results. **f**, Number of cells per integration site at P7. Each point represents one oligoclone. $AP_{15\rightarrow12}$ data has been reproduced from Fig. 3g for direct comparison. Values are shown as mean ± s.e.m.; $n = 39$ oligoclones ($AP_{15\rightarrow12}$), 17 oligoclones ($IP_{15\rightarrow12}$). **g**, $IP_{15\rightarrow12}$ daughter neurons express CUX1 but not CTIP2. Photomicrographs showing pattern of expression of CUX1 and CTIP2 are reproduced from Fig. 2. Values are shown as mean ± s.e.m.; $N = 2$ experimental litters (CUX1), 3 experimental litters (CTIP2). In **b**, vertically aligned cells belong to single integration sites. FT, FlashTag; IZ, intermediate zone.

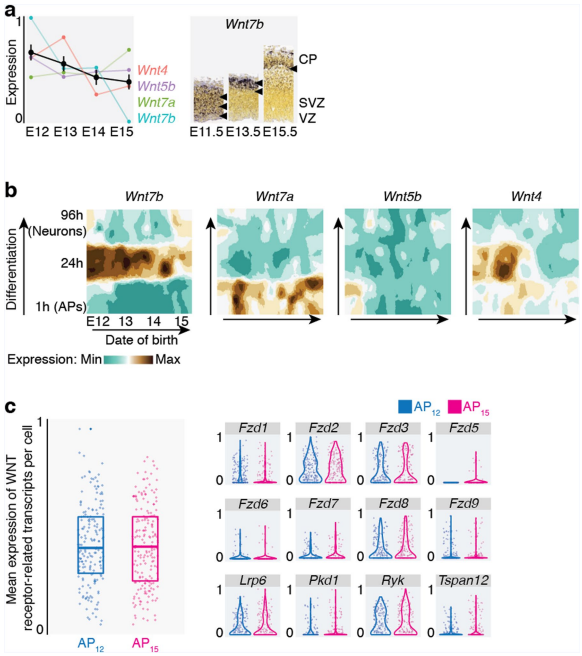

Extended Data Fig. 9 | Temporal dynamics of Wnt signalling in the developing cortex. a, Top, temporally dynamic expression of Wnt transcripts in the developing cortex (data from www.unige.ch/genebrowser.unige.ch/telagirdon)[8]. Values are shown as mean ± s.e.m.; $n = 189$ APs, 268 neurons (E12), 207 APs, 223 neurons (E13), 134 APs, 219 neurons (E14), 301 APs, 213 neurons (E15). Right, example of corresponding in situ hybridizations from the Allen Developing Mouse Brain Atlas (© 2008 Allen Institute for Brain Science. Allen Developing Mouse Brain Atlas. Available from: http://developingmouse.brain-map.org/). **b**, Dynamic expression of Wnt transcripts in the developing cortex (expression landscapes from www.unige.ch/genebrowser.unige.ch/telagirdon)[8]. The overall pattern is early–high to late–low (**a**). **c**, AP_{15} express Wnt receptor-related transcriptional programs (data from ref. [8]). Box plots indicate median and interquartile range. Right, expression of individual receptor-related transcripts in AP_{12} and AP_{15}. $n = 189$ APs (E12), 301 APs (E15).

Extended Data Table 1 | Selection of genes from the AP_{15} versus $AP_{15\rightarrow12}$ model

Gene symbol	Enriched in	Gene weight	Function	Reference (PMID)
Nav1	AP_{15}	1.23	Microtubule-associated protein involved in neuronal differentiation and migration	15797708
Tnc	AP_{15}	1.23	Extracellular matrix protein, regulates proliferation and differentiation in spinal cord neural progenitors and switch from neurogenesis to gliogenesis	15226258
Mfge8	AP_{15}	1.18	Regulates quiescence and neurogenesis in adult neural stem cells	30174295 / 30193126
Scmh1	AP_{15}	1.15	Chromatin modifier, dynamically expressed during developmental transitions in early embryogenesis	26403153
Pbx1	AP_{15}	1.13	Transcriptional activator; required for adult SVZ neurogenesis	27226325
Mmd2	AP_{15}	1.12	Putative mitochondrial protein, with known role in glial precursor maintenance and differentiation in the embryonic spinal cord	22500632
Igsf3	AP_{15}	1.12	Regulates neuronal morphogenesis	27328461
Cst3	AP_{15}	1.11	Supports differentiation of ES cells into neural stem cells, expressed in astrocyte progenitors	16595632 / 17064358 / 11144350
Flrt2	AP_{15}	1.08	FGF signaling regulator	16872596
Hdac3	$AP_{15\rightarrow12}$	-0.84	Histone deacetylase, required for proliferation of adult neural stem cells	25161285
Rcor2	$AP_{15\rightarrow12}$	-0.87	Co-repressor of histone demethylase LSD1, involved in neural progenitor proliferation regulation	26795843
Kat7	$AP_{15\rightarrow12}$	-0.87	Histone acetyltransferase, involved in maintenance of pluripotency and self-renewal in embryonic stem cells	25743411
Slc1a2	$AP_{15\rightarrow12}$	-0.92	Glutamate transporter, expression developmentally regulated	15804404
Ezh2	$AP_{15\rightarrow12}$	-0.98	Histone methyltransferase, regulates balance of proliferative *vs.* neurogenic divisions in neural progenitors	25989023 / 24553933
Vars	$AP_{15\rightarrow12}$	-1.04	Valyl-TRNA Synthetase, LOF linked to microcephaly	29691655
Tcf7l1	$AP_{15\rightarrow12}$	-1.09	Wnt pathway regulator, regulates balance of proliferative *vs.* neurogenic divisions in neural progenitors	21932308 / 19718027
Hist1h4d	$AP_{15\rightarrow12}$	-1.11	Histone protein	21605641
Chac1	$AP_{15\rightarrow12}$	-1.24	Notch signaling regulator	24767995

nature research

Corresponding author(s): Denis Jabaudon

Last updated by author(s): Jun 29, 2019

Reporting Summary

Nature Research wishes to improve the reproducibility of the work that we publish. This form provides structure for consistency and transparency in reporting. For further information on Nature Research policies, see Authors & Referees and the Editorial Policy Checklist.

Statistics

For all statistical analyses, confirm that the following items are present in the figure legend, table legend, main text, or Methods section.

n/a	Confirmed	
☐	☒	The exact sample size (*n*) for each experimental group/condition, given as a discrete number and unit of measurement
☐	☒	A statement on whether measurements were taken from distinct samples or whether the same sample was measured repeatedly
☐	☒	The statistical test(s) used AND whether they are one- or two-sided *Only common tests should be described solely by name; describe more complex techniques in the Methods section.*
☒	☐	A description of all covariates tested
☐	☒	A description of any assumptions or corrections, such as tests of normality and adjustment for multiple comparisons
☐	☒	A full description of the statistical parameters including central tendency (e.g. means) or other basic estimates (e.g. regression coefficient) AND variation (e.g. standard deviation) or associated estimates of uncertainty (e.g. confidence intervals)
☐	☒	For null hypothesis testing, the test statistic (e.g. *F*, *t*, *r*) with confidence intervals, effect sizes, degrees of freedom and *P* value noted *Give P values as exact values whenever suitable.*
☒	☐	For Bayesian analysis, information on the choice of priors and Markov chain Monte Carlo settings
☒	☐	For hierarchical and complex designs, identification of the appropriate level for tests and full reporting of outcomes
☒	☐	Estimates of effect sizes (e.g. Cohen's *d*, Pearson's *r*), indicating how they were calculated

Our web collection on statistics for biologists contains articles on many of the points above.

Software and code

Policy information about availability of computer code

Data collection	ImageJ version 2.0.0-rc-69/1.52n R version 3.5.0 R packages: ccRemover (V1.0.4), bmrm (V3.7), GenomicRanges (V1.32.7) STAR aligner version 2.5.3a.
Data analysis	BDFACSDiva software Illumina Hiseq 4000

For manuscripts utilizing custom algorithms or software that are central to the research but not yet described in published literature, software must be made available to editors/reviewers. We strongly encourage code deposition in a community repository (e.g. GitHub). See the Nature Research guidelines for submitting code & software for further information.

Data

Policy information about availability of data

All manuscripts must include a data availability statement. This statement should provide the following information, where applicable:

- Accession codes, unique identifiers, or web links for publicly available datasets
- A list of figures that have associated raw data
- A description of any restrictions on data availability

The datasets used in this study are available in the GEO repository under accession number GSE122644.

Field-specific reporting

Please select the one below that is the best fit for your research. If you are not sure, read the appropriate sections before making your selection.

☒ Life sciences ☐ Behavioural & social sciences ☐ Ecological, evolutionary & environmental sciences

For a reference copy of the document with all sections, see nature.com/documents/nr-reporting-summary-flat.pdf

Life sciences study design

All studies must disclose on these points even when the disclosure is negative.

Sample size	Sample size was not determined in advance but corresponds to what is being used in the field. Based on consistency of results between litters and between pups within a given litter, a sample size of 3-5 litters was considered sufficient.
Data exclusions	Only oligoclones containing neurons were quantified. This is mentioned in the methods. Exclusion criteria were pre-established.
Replication	Transplantations were performed both within and across litters and the oligoclonal analysis reveals a high degree of replicability across cells and animals.
Randomization	Does not apply. Experiments of different conditions were performed on different days based on animal availability.
Blinding	Blinding was used for data collection and analysis of pharmacological treatments in in vitro experiments. Blinding was not performed in other experiments due to the unambiguous nature of measurements and systematic analyses used in these experiments.

Reporting for specific materials, systems and methods

We require information from authors about some types of materials, experimental systems and methods used in many studies. Here, indicate whether each material, system or method listed is relevant to your study. If you are not sure if a list item applies to your research, read the appropriate section before selecting a response.

Materials & experimental systems

n/a	Involved in the study
☐	☒ Antibodies
☒	☐ Eukaryotic cell lines
☒	☐ Palaeontology
☐	☒ Animals and other organisms
☒	☐ Human research participants
☒	☐ Clinical data

Methods

n/a	Involved in the study
☒	☐ ChIP-seq
☐	☒ Flow cytometry
☒	☐ MRI-based neuroimaging

Antibodies

Antibodies used

Rat anti-CTIP2 (1:500; Abcam, #AB18465, LOT: GR322373-7);
rabbit anti-CUX1 (1:500; Santa Cruz; sc-13024, LOT: E2314);
rabbit anti-dsRed (1:1000; Clonetech; # 632496, LOT: 1612022);
mouse anti-GFAP (1:500; Sigma, #G3893)
rabbit anti-KI67 (1:250; Abcam, #AB15580, LOT: GR309960-2);
rabbit anti-NEUROD2 (1:1000; Abcam, #AB104430, LOT: GR118831-6);
rat anti-RFP (1:500; Chromotek; # 5F8, LOT: 60706002AB);
goat anti-SOX2 (1:500; SC Biotech, #SC17320);
mouse anti-SOX2 (1:500; Santa Cruz; sc-365823, LOT: G0717);
rabbit anti-SOX2 (1:500; Abcam; #AB97959, LOT: GR128998-1);
rabbit anti-TBR1 (1:500; Abcam; # AB31940, LOT: GR3182037-1);
rabbit anti-TBR2 (1:500; Abcam; ab23345, LOT: GR305614-10);
rat anti-TBR2 (1:500; Invitrogen, #14-4875-82, LOT: 4348755)

Validation

all antibodies used are commonly used in the field and have been validated in previous publications/by the manufacturer.
References and manufacturer validations can be found here:
Rat anti-CTIP2 (Abcam, #AB18465): https://www.abcam.com/ctip2-antibody-25b6-chip-grade-ab18465.html
rabbit anti-CUX1 (Santa Cruz; sc-13024): https://www.scbt.com/scbt/product/cdp-antibody-m-222
rabbit anti-dsRed (1:1000; Clonetech; # 632496, LOT: 1612022);
mouse anti-GFAP (1:500; Sigma, #G3893): https://www.sigmaaldrich.com/catalog/product/sigma/g3893?lang=de&region=CH
rabbit anti-KI67 (1:250; Abcam, #AB15580): https://www.abcam.com/ki67-antibody-ab15580.html
rabbit anti-NEUROD2 (1:1000; Abcam, #AB104430): https://www.abcam.com/neurod2-antibody-ab104430.html
rat anti-RFP (1:500; Chromotek; # 5F8): https://www.chromotek.com/products/detail/product-detail/rfp-antibody-5f8/

goat anti-SOX2 (1:500; SC Biotech, #SC17320): https://www.scbt.com/scbt/product/sox-2-antibody-y-17
mouse anti-SOX2 (1:500; Santa Cruz; sc-365823): https://www.scbt.com/scbt/product/sox-2-antibody-e-4
rabbit anti-SOX2 (Abcam; #AB97959): https://www.abcam.com/sox2-antibody-ab97959.html
rabbit anti-TBR1 (1:500; Abcam; # AB31940): https://www.abcam.com/tbr1-antibody-ab31940.html
rabbit anti-TBR2 (1:500; Abcam; ab23345): https://www.abcam.com/tbr2-eomes-antibody-chip-grade-ab23345.html
rat anti-TBR2 (1:500; Invitrogen, #14-4875-82): https://www.thermofisher.com/antibody/product/EOMES-Antibody-clone-Dan11mag-Monoclonal/14-4875-82

Animals and other organisms

Policy information about studies involving animals; ARRIVE guidelines recommended for reporting animal research

Laboratory animals	Mus musculus (CD1 strain; CAG::mRFP1 ((B6.Cg-Tg(CAG-mRFP1)1F1Hadj/J, JAX 005884) crossed with CD1 mice for at least 10 generations), E12.5, E15.5 and E17.5 embryos were used (both male and female)
Wild animals	The study did not involve wild animals.
Field-collected samples	The study did not involve field-collected samples.
Ethics oversight	All experimental procedures were approved by the Geneva Cantonal Veterinary Authorities, Switzerland.

Note that full information on the approval of the study protocol must also be provided in the manuscript.

Flow Cytometry

Plots

Confirm that:

☒ The axis labels state the marker and fluorochrome used (e.g. CD4-FITC).

☒ The axis scales are clearly visible. Include numbers along axes only for bottom left plot of group (a 'group' is an analysis of identical markers).

☒ All plots are contour plots with outliers or pseudocolor plots.

☒ A numerical value for number of cells or percentage (with statistics) is provided.

Methodology

Sample preparation	Apical progenitors were labeled by injection of FlashTag (FT) in the ventricle of embryos; the dorsal pallium was dissected and labeled progenitors were isolated by collecting the top 5-10% brightest FT-labeled cells.
Instrument	S3e Cell Sorter (BioRad) or a BD FACS Aria II flow cytometer (BD Biosciences)
Software	BDFACSDiva software
Cell population abundance	5-10%, determined by FT intensity
Gating strategy	The top 5-10% brightest cells were collected. Doublets and debris were exluded based on FSC and SSC.

☒ Tick this box to confirm that a figure exemplifying the gating strategy is provided in the Supplementary Information.